1

High mannose N-glycans on red blood cells as phagocytic ligands, mediating both sickle cell anaemia and resistance to malaria

Huan Cao[1], Aristotelis Antonopoulos[2], Sadie Henderson[3], Heather Wassall[1], John Brewin[4], Alanna Masson[5], Jenna Shepherd[1], Gabriela Konieczny[1], Bhinal Patel[2], Maria-Louise Williams[1], Adam Davie[1], Megan A Forrester[1], Lindsay Hall[1], Beverley Minter[1], Dimitris Tampakis[6], Michael Moss[3], Charlotte Lennon[1], Wendy Pickford[1], Lars Erwig[1], Beverley Robertson[2], Anne Dell[4], Gordon D. Brown[1,7], Heather M. Wilson[1], David C. Rees[4], Stuart M. Haslam[2], J. Alexandra Rowe[8], Robert N. Barker[*1], Mark A. Vickers[*1,3,5]

[1]School of Medicine, Medical Sciences and Nutrition, University of Aberdeen, U.K.

[2]Department of Life Sciences, Imperial College London, U.K.

[3]Scottish National Blood Transfusion Service, Aberdeen, U.K.

[4]Department of Haematology, King's College Hospital, London, U.K.

[5]Department of Haematology, Aberdeen Royal Infirmary, Aberdeen, U.K.

[6]Centre for Biological Engineering, School of Mechanical, Electrical and Manufacturing Engineering, Loughborough University and Division of Cancer Studies, King's College London, U.K.

[7]Medical Medical Research Council Centre for Medical Mycology at the University of Exeter.

[8]Centre for Immunity, Infection and Evolution, Institute of Immunology and Infection Research, University of Edinburgh, U.K.

*These authors contributed equally to this work

Abstract

In both sickle cell disease (SCD) and malaria, red blood cells (RBCs) are phagocytosed in the spleen, but receptor-ligand pairs mediating uptake have not been identified. Here, we report that patches of high mannose N-glycans ($Man_{5-9}GlcNAc_2$), expressed on diseased or oxidized RBC surfaces, bind the mannose receptor (CD206) on phagocytes to mediate clearance. Extravascular haemolysis in SCD correlates with high mannose glycan levels on RBCs. Infection of RBCs with *Plasmodium falciparum* expose surface mannose N-glycans on healthy RBCs, which occurred at significantly higher levels on RBCs from subjects with sickle cell trait compared to those lacking haemoglobin S. The glycans were associated with high molecular weight complexes and protease-resistant, lower molecular weight fragments containing spectrin. Recognition of surface N-linked high mannose glycans, a novel response to cellular stress, is the first molecular mechanism common to both the pathogenesis of SCD and resistance to severe malaria in sickle cell trait.

Introduction

Sickle cell disease (SCD) comprises a group of disorders affecting over 20 million individuals and is caused by a mutation causing an amino acid substitution (E6V) in the adult haemoglobin β chain (1, 2), so that the physiological haemoglobin (Hb) A tetramer, $\alpha_2\beta_2$, is replaced by the HbS tetramer $\alpha_2\beta^S_2$, which can form pathological polymers. The disease is variable, with modifiers such as high levels of the fetal β haemoglobin chain, γ, resulting in $\alpha_2\gamma_2$ or $\alpha_2 \beta^S\gamma$ tetramers that terminate HbS polymers and ameliorate disease. Milder disease is also associated with compound heterozygosity of the sickle cell allele with quantitative defects in α or β chains (thalassaemias) or other haemoglobin chain variants like haemoglobin C.

SCD is characterized by a multi-system vasculopathy and haemolysis, which cause much morbidity and mortality, especially in Africa. The anaemia has been ascribed to abnormal physical properties of diseased red blood cells (RBCs), which interfere with their transit through the splenic and hepatic vasculatures, so stimulating phagocytic uptake by tissue macrophages (3). However, the observation that isolated macrophages take up SCD RBCs selectively *in vitro* (4) indicates the presence of disease-specific ligands, which remain uncharacterized. Heterozygosity for HbS, sickle cell trait (SCT), affects over 250 million individuals and is maintained in the population by conferring protection against severe malaria. The mechanism underlying this protection is not fully explained, but the mutation has long been known to prevent high levels of parasitaemia (5, 6). Yet under most conditions *in vitro*, the parasites grow equally well in SCT RBCs compared to those with normal haemoglobin (7, 8), implying that protection is due to

60   efficient immune clearance of infected SCT RBCs, and again raising questions as to the identity

61   of the ligands responsible for mediating phagocytosis.

62

63   ## Results

64

65   **Red blood cells from patients with SCD express high mannose N-glycans on their surfaces**

66

67   We postulated these putative uptake ligands might be N-linked glycans, given the prominence of

68   the glycocalyx on RBCs and the corresponding expression of lectins as key innate receptors on

69   macrophages (9). A survey for surface ligands using a panel of plant lectins identified two panel

70   members that bound preferentially to SCD RBC (Fig. 1a), *Galanthus nivalis* Agglutinin (GNA)

71   and *Narcissus pseudonarcissus* Lectin (NPL). Binding was specific (Extended Data Table 1,

72   Extended Data Figs. 1a-b, 2a) and both lectins were noted to have similar specificities for

73   terminal mannose residues (Extended Data Fig. 1a) (10, 11). Microscopy with fluorescent GNA

74   lectin revealed discrete patches on the surfaces of SCD (HbSS), but not healthy (HbAA), RBCs

75   (Fig. 1b, Extended Data Fig. 1c, d). Glycomic analysis using mass spectrometry showed that

76   SCD RBCs express N-linked high mannose glycans, hereafter high mannose glycans (Man_{5-}

77    $_9GlcNAc_2$; Fig. 1c), which are known ligands for phagocytosis by macrophages (9, 12) and

78   therefore good candidates for mediating RBC uptake. High mannose glycans are also observed in

79   the N-glycome profiles from HbAA RBC ghosts (Fig. 1c, Extended Data Fig. 3, Extended Data

80   File 1). The proportions of high mannose glycans with respect to whole N-glycomes were not

81   significantly different between sickle and healthy RBC ghosts (Extended Data Fig. 1e). The

82   marked difference between GNA binding on the cell surface of HbAA compared to HbSS RBCs

83   is therefore not explained by the total high mannose glycan content of the ghosts.

84

85   **RBC surface mannose correlates with extravascular haemolysis in sickle cell disease**

86

87   To assess the relevance of high mannose N-glycan display for RBC uptake *in vivo*, we exploited

88   the heterogeneity of SCD arising from the interactions of HbS with other mutations in the globin

89   loci (such as HbC, α- and β-thalassaemias) that also protect against malaria (13). If mannoses

90   were phagocytic ligands in SCD, higher levels of mannose exposure should correlate with more

91   severe anaemia. Despite a similar glycomic profile, RBCs from patients who were homozygous

92   for HbS (HbSS) tended to exhibit higher binding of GNA lectin, compared to RBCs from healthy

93   individuals containing HbAA or those with SCT (HbAS) (Fig. 2a). Patients with SCD who were

94   compound heterozygotes for HbS and either HbC or β-thalassaemia, or who had HbSS but with

95   mitigating α-thalassaemia or high levels of HbF, tended to exhibit low to intermediate GNA

96   lectin binding (Fig. 2a). RBCs in other anaemias did not express high levels of exposed mannose

97   residues (Extended Data Fig. 2a). The classical apoptotic marker for phagocytosis,

98   phosphatidylserine, as measured by annexin V binding, was expressed at similar, low levels on

99   RBCs from each of the clinical groups (Extended Data Fig. 2b), although it was highly expressed

100   on positive control calcium ionophore treated, eryptotic RBCs (Extended Data Fig. 2c). Overall,

101   GNA lectin binding correlated significantly with more severe anaemia (Fig. 2b) and other

102   markers of haemolysis (Extended Data Fig. 2d, e), consistent with high mannose N-glycan

103   expression driving 'extravascular' uptake by hepatosplenic phagocytes, which is the major

104   mechanism of haemolysis in SCD (14). A minor, but significant, proportion of RBC loss in SCD

105   is also accounted for by intravascular haemolysis (14). However, plasma lactate dehydrogenase

106   (LDH) levels, a marker of intravascular haemolysis (14), did not correlate with RBC GNA lectin

107   binding (Fig. 2c, d, e) within HbSS patients. We postulated that mannose binding lectin might

108   bind and opsonize sickle cells, but no significant correlations between levels of this plasma

109   protein and haemolytic phenotypes were observed (Extended Data Fig. 4a-c). Furthermore, when

110   we added cells washed free of plasma to macrophages, SS, but not AA, RBCs were selectively

111   taken up and this could be inhibited by mannan (Fig. 2f), indicating the macrophages expressed a

112   receptor that interacted directly with surface mannoses.

113

114   **Surface mannoses can be induced on healthy RBC by oxidative stress and are recognized**

115   **by the mannose receptor (CD206)**

116

117   High mannose N-glycans ($Man_{5-9}GlcNAc_2$) were detected in glycomic analyses of healthy

118   (HbAA) RBCs (Fig 1c, Extended Data Fig. 3). Furthermore, permeabilization of healthy RBCs

119   allowed GNA lectin binding in patches that colocalized with the membrane skeleton (Extended

120   Data Fig. 5a). SCD is associated with intracellular oxidative stress (15, 16), so we determined

121   whether exposing healthy RBCs to an oxidizing agent (Extended Data Fig. 5b) would alter the

122   surface mannose exposure as assessed by GNA lectin binding (Fig. 3a). Under the experimental

123   conditions applied, oxidation of healthy RBCs indeed resulted in binding of GNA lectin, with

124   similar, but fewer, patches observed compared to unoxidized HbSS RBCs (Fig. 3b). Artefactual

125   GNA lectin-binding resulting from permeabilization of the cell by oxidative damage was ruled

126   out (Extended Data Fig. 5c), as was potential intracellular O-GlcNAc binding by GNA lectin

127   (Extended Data Fig. 5d). To identify the cognate receptor on macrophages, we measured the

128   binding of a panel of recombinant mammalian C-type lectin fusion proteins with different glycan

129   specificities to oxidized RBCs. This survey implicated the mannose receptor (17, 18) (MR,

130   CD206), in particular the mannose recognizing carbohydrate recognition domain (MR-CRD)

131   (Fig. 3c). We also observed that in cultures of oxidized RBCs with human monocyte derived

132   macrophages (HMDM) *in vitro*, uptake was restricted to MR positive cells (Fig. 3d).

133   Furthermore, siRNA knockdown of MR in macrophages (Extended Data Fig. 6c) specifically

134   reduced phagocytosis (Fig. 3e, Extended Data Fig. 6d); and phagocytosis was also inhibited by

135   the competing glycans mannan or chitin, each known to block MR-CRD (19), but not inhibited

136   by the control glycan laminarin (Fig. 3f, Extended Data Fig. 6e). Finally, MR-CRD-blocking

137   antibody also inhibited phagocytosis of both oxidized healthy and native SCD RBC (Fig. 3g, h),

138   which was also sensitive to mannan and chitin (Fig. 3i). Taken together, these results

139   demonstrate that phagocytosis of mannose-displaying RBC is dependent on MR, although

140   involvement of other receptors cannot be excluded.

141

142   **GNA lectin binding proteins comigrate with spectrin containing complexes**

143

144   The above data show that high mannose sugars occur in the glycomes of both HbAA and HbSS

145   RBC, and that these sugars can be detected on the surface of HbSS RBC and oxidized HbAA

146   RBC by GNA lectin binding. To identify the proteins carrying the high mannose sugars, extracts

147   of HbAA and HbSS RBC membranes were analysed by western blots probed with GNA lectin.

148   A GNA-binding doublet around 260kDa was identified in both HbAA and HbSS RBC (Fig. 4a),

149   which is similar in molecular weight to the abundant membrane skeleton proteins α- and β-

150   spectrin. Blots of HbSS ghosts showed additional GNA lectin-binding bands at ~160kDa,

151   ~100kDa, ~70kDa and ~50kDa, which were not seen in fresh HbAA and HbAS RBC (Fig. 4a-b).

152   When HbAA RBCs were stored for six weeks, to allow oxidative damage to membrane skeletal

153   proteins (20), lower molecular weight Endo-H (N-glycan specific glycosidase) sensitive GNA

154   lectin-binding bands corresponding in size to fragments seen in HbSS cells were seen on western

155   blotting, and GNA lectin precipitation enriched these fragments (Extended Data Fig. 7a, b). The

156   intensity of the 100kDa fragment was noted to correlate positively with RBC surface GNA lectin

157   binding assessed by flow cytometry (Fig. 4b, Extended Data Fig. 7c), suggesting a role in the

158   surface exposure of high mannose glycans. The specificity of the GNA lectin binding was

159   confirmed by treating RBC ghosts with N-glycan specific glycosidases (PNGase F and Endo-H)

160   prior to western blotting, which abolished GNA-binding to all of the above bands (Fig. 4c). We

161   next attempted to determine whether treatment of RBC ghosts with N-glycanases reduced the

162   sizes of GNA-binding bands. A molecular weight change was not observable for the high

163   molecular weight doublet around 260kDa, although the large sizes of these proteins made minor

164   shifts in difficult to observe. However, a ~70kDa band from HbSS ghosts did show an

165   appropriate reduction in molecular weight, consistent with cleavage of N-glycans after treatment

166   of RBC ghosts with PNGase F and Endo-H (Fig. 4d). Western blotting with antibodies to β-

167   spectrin, indicated the band contained an epitope derived from spectrin.

168

169   To investigate the association of spectrin with high mannose glycans species further, we carried

170   out mass spectrometric analysis of tryptic peptides from the 260kDa GNA-binding doublet from

171   both HbAA and HbSS RBC ghosts and found that both bands contained large quantities of α-

172   and β-spectrin (Extended Data Table 2). As has been previously reported in RBC proteomic

173   experiments (21), other abundant RBC proteins of lower molecular weight were also identified,

174 including integral membrane glycoproteins such as Band 3 and Glut-1 (Extended Data Table 2).

175 However, despite extensive mass spectrometric analyses from the 260 kDa doublet, no

176 conventionally glycosylated peptides were identified.

177

178 Further evidence indicating covalent linkages between high mannose glycan containing

179 glycoproteins/glycopeptides and spectrin derived peptides came from western blots of membrane

180 extracts from HbSS RBC or HbAA ghosts treated with trypsin, which exhibited anti-spectrin

181 binding lower molecular weight bands comigrating with GNA lectin signals (Extended Data Fig.

182 7c, d), particularly marked for the 50kDa GNA-binding band and α-spectrin antibodies. GNA

183 lectin precipitation of extracts from HbAA ghosts followed by western blotting with antibodies

184 to spectrin, detected a ~260 kDa protein (Fig. 4e). Finally, super resolution imaging of

185 permeabilized HbAA and HbSS RBC demonstrated GNA lectin co-localising with spectrin in

186 discrete patches scattered in the spectrin membrane skeletal network (Fig. 4f). Taken together

187 these data support the hypothesis that spectrin containing complexes in HbSS and oxidized

188 HbAA RBCs are N-glycosylated with high mannose glycans, although it was not possible to

189 detect specific N-glycosylated peptides through conventional glycoproteomic approaches.

190

191 **GNA lectin binds to low molecular weight complexes that include spectrin, are protease**

192 **resistant and derive from higher molecular weight aggregates**

193

194 In order to generate smaller fragments of high mannose-bearing fragments that would be more

195 amenable to characterization, HbSS ghosts were incubated with serial dilutions of trypsin,

196 spectrin was purified from them and then probed with GNA in western blots. This showed that

197   high concentrations of trypsin, sufficient to digest the 260kDa and 160kDa GNA lectin binding

198   proteins, failed to degrade the ~50kDa, ~70kDa and ~100kDa GNA lectin binding gel bands

199   (Fig. 4g and Extended Data Fig. 7e)). Indeed, the intensities of these bands, particularly that at

200   ~100kDa, increased with higher trypsin concentrations (Fig. 4g). Prolonged, high concentration

201   trypsin digestion eventually degraded the ~100kDa fragment, and, to some extent, the ~70kDa

202   GNA lectin binding bands, with concurrent appearance of a new GNA lectin binding band

203   around 40kDa, which we term F40 (Extended Data Fig. 7f). This same pattern of loss of the

204   ~100kDa and ~70kDa GNA lectin binding fragments with concurrent appearance of F40 was

205   also observed when HbSS erythrocytes were stored over five weeks (Extended Data Fig. 7g).

206   Hence, protease digestion results in formation of a 40kDa protease-resistant fragment that binds

207   GNA lectin and therefore carries high mannose glycans.

208

209   The F40 fragment was concentrated through sequential 100kDa and 10kDa cut-off concentrators

210   (Extended Data Fig. 8a, b), and the resulting band cut out from a gel for glycoproteomic analysis.

211   Proteomic analysis of F40 identified peptides from α-spectrin, particularly the N-terminal 370

212   amino acids (Fig. 4h, Extended Data Table 3). PNGase-F treatment of the purified F40 fragment

213   released N-glycans consisting mainly of high mannoses (Man_6-Man_9) and complex structures

214   (Extended Data Fig. 8c). However, once again, no specific glycopeptides could be identified. We

215   postulated that the reason for this, and the relatively low identified protein sequence coverage,

216   could be unconventional peptide structures arising from oxidized and glycated aggregates.

217   Indeed, mass spectrometry confirmed the presence of lysine glycation in α-spectrin peptides

218   from F40 at amino acids K59, K270 and K281. Furthermore, although GNA lectin binding to

219   F40 was Endo-H sensitive, the enzyme required denaturing conditions to be effective (Fig. 4i),

220 consistent with the possibility of protein aggregates. Additionally, the N-terminal α-spectrin

221 antibody, B12, failed to bind to the full-length F40 band, but bound to smaller fragments after

222 treatment with a combination of proteases, indicating a cryptic epitope (Extended Data Fig. 8d, e,

223 f). Finally, when visualized in 3D-SIM, some HbSS cells show large aggregates of intracellular

224 spectrin, which correspond to dense GNA lectin surface staining (Fig. 4j). Overall, our data

225 demonstrate the existence of high mannose glycans in HbSS RBC extracts and suggest that the

226 main GNA lectin-binding molecules are spectrin-containing glycoprotein complexes with

227 atypical structures, including glycated forms, that make analysis by conventional

228 glycoproteomics challenging.

229

230 **Infection of RBCs with *P. falciparum* causes exposure of high mannose N-glycans,**

231 **especially those from donors with SCT**

232

233 As infection of RBC with malarial parasites is associated with oxidative stress (22), we

234 investigated whether exposure of high mannose N-glycans might be important in protection

235 against infection with *P. falciparum*, particularly in the context of SCT. First, we determined the

236 sensitivity of SCT RBCs to a given oxidative stress and found they bound more GNA lectin than

237 HbAA RBC (Fig. 5a). Interestingly, the proportion of HbS correlated well with the degree of

238 oxidative stress (Fig. 5b). These data suggested that exposure of high mannose N-glycans might

239 contribute to the resistance of individuals with SCT to severe malaria, by enhancing clearance of

240 infected cells. We therefore infected HbAA and HbAS RBC with *P. falciparum* and assessed

241 high mannose N-glycan exposure as the infection progressed through ring, trophozoite and

242 schizont stages. HbAA RBCs containing schizonts, but not trophozoites, expressed significantly

243   higher exposed high mannose N-glycans as indicated by increased GNA lectin binding (Fig. 5c).

244   Importantly, HbAS RBCs containing schizonts expressed even higher levels of exposed high

245   mannose N-glycans and this increased expression extended into the trophozoite stages (Fig. 5c).

246   *P. falciparum* infected RBCs cytoadhere to vascular endothelium, to avoid phagocytosis by

247   hepatosplenic macrophages (23, 24), and this adhesion is mediated by the expression of PfEMP1

248   on late stage infected RBC (25). Reduced display of PfEMP1 on the surface of HbAS-infected

249   RBCs is a potential mechanism of protection against malaria in SCT (26), and PfEMP1 levels

250   show considerable variation in different HbAS donors (27). We therefore determined PfEMP1

251   expression in addition to mannose display and noted a marked inverse correlation (Fig. 5d).

252

253

254   **Discussion**

255

256   This work has identified a novel receptor-ligand pair mediating RBC clearance that underlies

257   both the extravascular haemolysis of SCD and clearance of *P. falciparum* infected

258   RBCs. Immunologically, the latter can be regarded as protective immunity arising from

259   recognition of altered self, with the mannose receptor recognizing a pattern common to both

260   diseased and infected cells. Display of high mannose N-glycans on membrane proteins could

261   also be regarded as a new damage-associated molecular pattern (DAMP). The mannose receptor

262   is expressed in human spleens by Lyve-1+ cells lining venous sinuses, where they form a

263   physical barrier for blood cells to exit the red pulp and so are ideally located to perform a

264   filtering function (28). In infection with *P. falciparum*, the parasite evades passage through the

265   spleen by expressing adhesive proteins, notably PfEMP1, on the surface of infected RBCs, so

266   that they adhere to endothelial cells in the systemic circulation. The inverse correlation between

267   mannose exposure and surface PfEMP1 implies similar processes involving oxidation induced

268   membrane skeletal rearrangements underlie both phenomena (29, 30). Reduced PfEMP1 in

269   infected HbAS RBCs will lead to a failure of cytoadherence, and the exposed high mannose N-

270   glycans on circulating infected RBC will induce clearance by hepatosplenic phagocytes.

271   Together with the spleen's role in processing high mannose N-glycan bearing RBCs in SCD,

272   these data are consistent with spleen being the primary organ in removing RBCs infected with

273   malaria exposing high mannose N-glycans. Our work also potentially sheds light on the reasons

274   why those with SCD are so susceptible to infections with encapsulated bacteria, especially

275   *Streptococcus pneumoniae*, which is the commonest cause of death in children (1). Capsular

276   polysaccharides from pneumococcus are known to bind the carbohydrate binding domains of the

277   mannose receptor (31). It therefore seems likely that the high mannose N-glycans on the surfaces

278   of sickle cells would compete with bacteria for uptake by the mannose receptor.

279

280   Our work has also identified a new phenomenon whereby complexes of membrane skeletal

281   proteins, and fragments derived from them, are associated with high mannose N-glycans, which

282   act as an eat me signal. There are still only two accepted eat me signals in higher eukaryotes,

283   phosphatidylserine and calreticulin (32). This work therefore adds a third ligand to perform this

284   role. The expression of ligands for uptake attached to the membrane skeleton would allow

285   receptors on phagocytic cells to bind to molecules with high tensile strength, which may be

286   important for capturing cells as they transit through the spleen under conditions of high shear

287   stress.

288

289   Protein aggregates are thought to form after attacks by free radicals, reactive oxygen and

290   nitrogen species and glycation. These result in a wide variety of amino acid adducts (33), some

291   of which mediate the cross-links thought to underlie the formation of aggregates. Complexes of

292   damaged proteins, including spectrin, secondary to oxidative damage associated with haemolysis

293   have long been recognized in RBCs (34-37), partly arising from interaction with free radicals

294   generated by denatured haemoglobin species (hemichromes), including in SCD (38). Oxidative

295   degradation has been shown to be one of the main causes of membrane skeletal protein

296   alterations occurring in RBCs in storage, with proteolytic cleavage having a secondary role (20).

297   Interestingly, spectrin containing species were detected either as low molecular weight fragments

298   covering the N-terminus, as found in our proteomic analysis, or as high molecular aggregates

299   (20). Oxidation during the storage period of RBCs has also been shown to inactivate

300   glyceraldehyde 3-phosphate dehydrogenase, an important enzyme for ATP synthesis (20, 39). In

301   turn, this leads to dissociation of spectrin from the phosphatidylserine molecules of the RBCs

302   membrane, in an ATP dependent mechanism, resulting in increased spectrin-glycation products

303   (40).

304

305   Therefore, either by directly acting on the cytoskeletal proteins, or indirectly through ATP

306   dependent mechanisms, oxidative damage of RBCs is a mechanism that induces alterations in

307   membrane protein organization leading to aggregation of membrane glycoproteins. This is in

308   accordance with a recent report demonstrating that oxidative stress results in cluster-like

309   structures on the membrane of RBCs as a result of possible reorganization and aggregation (41).

310   RBCs contain various glycoproteins such as band 3, glycophorin, GLUT1, CD44 and CD47 (42).

311   Therefore, the enhanced phagocytosis we describe could potentially be driven by the aggregation

312   of RBC membrane glycoproteins increasing the local concentration of high mannose N-glycans,

313   thus favouring their recognition by the mannose receptor. This is in accordance with previous

314   reports showing that the binding affinity of the mannose receptor increases with the density of

315   mannose-containing glycoproteins (43). Taken together, we suggest that oxidative stress in RBCs

316   induces glycoprotein reorganization and aggregation, resulting in increased high mannose glycan

317   bearing densities that are recognized by the mannose receptor.

318

319   In summary, we describe a mechanism whereby oxidatively-damaged, membrane protein

320   complexes display high mannose N-glycans, which act as eat me signals important in the

321   haemolysis of sickle cell disease and resistance against severe malaria. It therefore represents the

322   first unified mechanism to explain both advantageous and deleterious consequences of the sickle

323   mutation.

324 # **Methods**

325 *Donors*

326 Ethical approval was obtained for the study (North of Scotland REC Number 11/NS/0026).

327 Further samples, including donors with SCT, were obtained from the NHS Grampian

328 Biorepository scheme (application number TR000142). Discarded anonymized samples were

329 also obtained from patients with SCD from King's College Hospital. HbAA, HbAS and SCD

330 statuses were assessed by Hb HPLC (Tosoh G7). All samples from patients were collected into

331 EDTA tubes (Becton-Dickinson).

332 *RBC isolation*

333 Blood was collected into acid citrate dextrose solution tubes (ACD; 455055, Grenier) and RBC

334 isolated by sodium metrizoate density gradient centrifugation (1.077 g/ml, Lymphoprep;

335 1114547 Axis-Shield). Packed RBC were diluted with an equal volume of Dulbecco's modified

336 Eagle's medium (DMEM; 4.5 g/L glucose, L-glutamine; 41965, Gibco), stored in ACD (9 ml

337 RBC/DMEM per ACD tube) at 4°C and used within 3 days unless otherwise stated.

338 *Lectins*

339 Biotinylated lectins were all purchased from Vector Laboratories. They include: *Galanthus*

340 *nivalis* Agglutinin (GNA, B-1245, 4μg/ml), *Narcissus pseudonarcissus* Lectin (NPL, B-1375,

341 4μg/ml), *Griffonia simplicifolia* Lectin II (G.Simp, B-1215, 4μg/ml), *Solanum tuberosum* Lectin

342 (STL, B-1165, 20 ng/ml), *Aleuria aurantia* Lectin (AAL, B-1395, 33ng/ml), *Maackia amurensis*

343 Lectin II (MAL II, B-1265, 67ng/ml), *Sophora japonica* Lectin (Vector Laboratories, no longer

344 available, 1μg/ml). FITC conjugated Peanut agglutinin was purchased from Sigma-Aldrich

345 (PNA, L7381-2MG, 2μg/ml).

346 *Flow cytometry*

347 Whole blood flow cytometry assays were used for Fig. 1a, 2, Extended Data Fig. 1a, 2, 3b, d, e

348 and 8a. Whole blood was washed first in phosphate buffered saline (PBS). Purified RBC were

349 used for the other flow cytometry experiments. RBC gating was applied by forward and side

350 scatter gating of both whole blood and purified RBC flow cytometry experiments (Extended

351 Data Fig. 9a). Staining with anti-glycophorin A (GPA) confirmed gates contained >99% RBC

352 (data not shown).

353 For lectin flow cytometry, approximately 5×10^6 RBC were washed three times in PBS, and

354 incubated for 15 minutes at room temperature in calcium buffer (10mM HEPES, 150mM $NaCl_2$,

355 2.5mM $CaCl_2$, pH 7.4) containing 10% Carbo-Free Blocking Solution (SP5040, Vector

356 Laboratories) for whole blood flow cytometry or just buffer alone for purified RBC flow

357 cytometry. Biotinylated lectin staining was carried out at room temperature in the same buffer as

358 the initial blocking step. PNA-FITC and other antibody staining was carried out in PBS

359 throughout, without contact with calcium buffer or Carbo-Free Blocking Solution. Lectin and

360 antibody staining were carried out for 30 minutes at room temperature, protected from light.

361 Annexin V staining was carried out according to the manufacturer's instructions (640945,

362 Biolegend). For biotinylated lectin staining, cells were then washed and incubated with

363 streptavidin PE-Cy7 (0.27 µg/ml; 25431782, eBioscience) or PE (0.67 µg/ml; 554061, BD

364 Pharmingen) for 30 minutes at room temperature. Humanized Fc fusions of murine C-type

365 lectins (17, 44) (5 µg/ml) were incubated with RBC for 30 minutes at room temperature in

366 calcium buffer, then detected by Alexa Fluor 647 goat anti-human secondary antibody (2 µg/ml;

367 109-605-098, Jackson ImmunoResearch Laboratories). In tests of their specificity for binding

368 RBC, lectin or Fc fusion proteins were first incubated with mannan (5 mg/ml, unless otherwise

18

369   stated) for 15 minutes at room temperature. Biotinylated BRIC 132 and BRIC 163 (10 µg/ml;

370   9458B and 9410B, International Blood Group Reference Laboratory) and anti-O-GlcNAc (1

371   µg/ml, RL2; 59624, Santa Cruz) binding to RBC were performed in PBS for 30 minutes at room

372   temperature, before incubation with streptavidin secondary (for BRIC 132/163) or anti-mouse PE

373   secondary (for anti-O-GlcNAc) for a further 30 minutes.

374   Prior to intracellular staining, RBC were fixed with glutaraldehyde (0.05%, 10 minutes, room

375   temperature), permeabilized with Triton X-100 (0.1% in PBS) for 5 minutes at room temperature

376   and then washed in PBS. Cells were washed before cytometric analysis. Data were acquired on a

377   FACSCalibur (BD) and analysed using FlowJo v10.0 (Treestar) software. Normalized geometric

378   mean fluorescences (gMFI) were calculated by subtracting the gMFI of secondary

379   antibody/streptavidin-only paired controls. For PNA-FITC and Annexin V analysis, unstained

380   controls were used for gMFI normalization.

381   *RBC ghost preparation*

382   Washed RBC were subjected to ice cold hypotonic lysis in 20 mM Tris, pH 7.6, with protease

383   inhibitor (05056489001, Roche) (45). Lysates were washed three times in hypotonic lysis buffer

384   (37000 g, 4°C, 30 minutes) before resuspension in minimal hypotonic lysis buffer. Protein

385   concentrations were determined by protein BCA assay (23227, Pierce). No trypsinization was

386   performed before any glycan analysis.

387   *Glycomic mass spectrometry (MS)*

388   N-linked glycan analysis from RBC ghosts were performed according to Jang-Lee *et al.* (46). MS

389   and MS/MS data from the permethylated purified glycan fractions were acquired on a 4800

390   MALDI-TOF/TOF mass spectrometer (Applied Biosystems). Data were processed using Data

391   Explorer 4.9 Software (Applied Biosystems). The processed spectra were subjected to manual

392 assignment and annotation with the aid of a glycobioinformatics tool, GlycoWorkBench (47).

393 Proposed assignments for the selected peaks were based on ^{12}C isotopic composition together

394 with knowledge of the biosynthetic pathways, and structures were confirmed by data obtained

395 from MS/MS experiments.

396 *Proteomics*

397 RBC ghost membranes were subjected to SDS-PAGE (10% Bis-Tris gel with MOPS running

398 buffer). SDS-gel bands a were excised, sliced into small pieces, and destained with 200 μl of 1:1

399 v:v acetonitrile:ammonium bicarbonate (50 mM, pH 8.4; AMBIC). Destained gel pieces were

400 then reduced by treatment with 10 mM DTT in AMBIC at 56 °C for 30 min, carboxymethylated

401 in 55 mM iodoacetic acid in AMBIC in the dark at room temperature, and then subjected to

402 overnight sequencing grade modified trypsin (Promega V5111) digestion in AMBIC at 37 °C.

403 After enzyme inactivation (100 °C water bath, 3 min), the digested peptides were extracted twice

404 from the gel pieces by incubating sequentially (15 min with vortexing) with 0.1% trifluoroacetic

405 acid and 100% acetonitrile. Finally, the volume was reduced with a Speed Vac. Eluted peptides

406 were analysed by LC–MS using a NanoAcquity UPLC™ system coupled to a Synapt™ G2-S

407 mass spectrometer (Waters MS Technologies, Manchester, UK) in positive ion mode. 5 μL of

408 sample was injected onto the analytical column (Waters, HSS T3, 75 μm × 150 mm, 1.8 μm).

409 Peptides were eluted according to the following linear gradient program (A: 0.1% v/v formic

410 acid in water, B: 0.1% v/v formic acid in acetonitrile): 0-90 min, 3-50% of B. MS data were

411 acquired on the Synapt G2-S using a data-dependent acquisition program, calibrated using Leu-

412 Enkephalin peptide standard. The top 20 components were selected for MS/MS acquisition.

413 Identification of the eluted peptides was performed using ProteinLynx Global SERVER™ v3.03

414 (Waters) using human porcine trypsin database (Uniprot 1.0). The following were set as

415   workflow parameters on PLGS: fixed carboxymethyl modification for cysteine, variable

416   deamidation and oxidation modifications for glutamine and methionine respectively.

417   *Human monocyte-derived macrophage (HMDM) preparation and culture*

418   Mononuclear cells were isolated by density centrifugation from whole blood and seeded at 10^6

419   cells/ml in Roswell Park Memorial Institute medium (RPMI (21875-034, Gibco)), 100 U/ml

420   penicillin, 100 µg/ml streptomycin, 292 µg/ml L-glutamine (10378-016, Gibco) and 10% heat

421   inactivated autologous serum. Cultures were incubated at 37°C with 5% CO_2 for 14-21 days.

422   Cells were washed with RPMI three times prior to use.

423   *Phagocytosis Assay*

424   For identification of phagocytosis by microscopy, RBC were stained with Cell Trace Far Red

425   (CTFR) (C34564, Molecular Probes) according to the manufacturer's instructions with minor

426   alterations: CTFR was diluted at 1 in 500 (2 μl/ml) in RPMI with penicillin and streptomycin

427   (RPMI/PS) media and incubated with 20 µl packed RBC for 30 minutes at 37°C, after which

428   staining was inhibited by adding 10% FCS (10270-106, Gibco). Stained cells were washed in

429   RPMI/PS prior to counting and addition to macrophages. RBC were added to HMDM at 5 x 10^7

430   cells per well for 3 hours, before removal of cells, washing and fixation with 4%

431   paraformaldehyde (Extended Data Fig. 6a). RBC bound, but not ingested, by HMDM were then

432   stained with anti-glycophorin-FITC (HIR2 antibody; 306610, Biolegend). Cells were imaged

433   using an immunofluorescence microscope (Zeiss AxioObserver Z1). Phagocytic macrophages

434   were defined as containing at least one CTFR-positive GPA-FITC-negative RBC (determined by

435   bright field). Three examples of oxidized RBC phagocytosis are shown in Extended Data Fig.

436   6b, marked 'P'. RBC-binding macrophages were defined as associated with at least one

437   glycophorin-FITC/CTFR double positive RBC. Analysis of HMDM phagocytosis included only

438   the small, non-granular subset of macrophages, because of consistent association with

439   phagocytosis and binding of RBC. For quantification of phagocytosis, 200-500 such

440   macrophages were counted per treatment. To test specificity of HMDM recognition, the

441   polymers mannan (10 mg/ml; M-7504, Sigma-Aldrich), chitin (50 μg/ml; C9752, Sigma-

442   Aldrich) or laminarin (10 mg/ml; L9634, Sigma-Aldrich), or anti-CD206 blocking antibody (10

443   µg/ml clone 15.2 321102, BioLegend; isotype control mouse IgG1 kappa clone 107.3; 554721,

444   BD Biosciences) were added to cultures 60 minutes before phagocytosis assays. Coumarin-

445   stained 6 µm Fluoresbrite carboxylate microspheres, of similar size to RBC, were used to assess

446   RBC independent phagocytosis (Extended Data Fig. 6e).

447   *RBC oxidation and eryptosis*

448   Purified RBC were incubated for 60 or 30 minutes respectively with 0.2 mM copper sulphate and

449   5 mM ascorbic acid at 37°C in DMEM with 4.5 g/L glucose. Cells were washed in PBS 3 times

450   prior to use. To induce eryptosis, calcium ionophore (2µM, A23187, Sigma-Aldrich) was applied

451   at 37°C in DMEM, with 4.5 g/L glucose, to purified RBC for 3 hours.

452   *Reactive Oxygen Species (ROS) Production*

453   The rate of ROS production was determined by first loading purified oxidized or untreated RBC

454   with oxidation sensitive dye CM-H2DCFDA (10 µM; C6827, Molecular Probes) in PBS and

455   incubating for 60 minutes in the dark at 37°C. RBC were then washed three times, resuspended

456   in DMEM and fluorescence determined immediately by spectrofluorimeter (Fluostar Optima;

457   BMG Labtech) with excitation of 485 nm and emission 530 nm. The rate of ROS formation was

458   calculated for the linear portion of the fluorescence/time curve generated over six hours, which

459   typically lasted for three hours.

460   *Lectin/Immuno-blotting*

461 Ghost preparations were mixed in equal volumes with SDS sample buffer containing 8M urea

462 (45) and heated at 100°C for 10 minutes. Ghost protein samples were fractionated by gel

463 electrophoresis using NuPage 4-12% Bis-Tris gel (Invitrogen, NP0312BOX) and transferred by

464 western blotting (30V, 1 hour) to polyvinylidene fluoride membrane (P 0.45 µm; 10600023

465 Amersham Hybond, GE Healthcare). Blots were probed with biotinylated GNA lectin (40 µg/ml;

466 B1245, Vector Laboratories) and Streptavidin HRP (1:2500 dilution, 3999S, Cell Signalling) in

467 calcium binding buffer (10mM HEPES, 150mM $NaCl_2$, 2.5mM $CaCl_2$, pH 7.4) containing 1x

468 Carbo-Free Blocking Solution (Vector Laboratories, SP-5040) and protease inhibitor cocktail

469 (11836145001, Roche) before development in Amersham ECL Select substrate (RPN2235, GE

470 Healthcare). 0.1% Tween-20 was added in probing and washing steps. Loading of wells was

471 normalized by protein concentration (~6 µg per sample). Enzymes PNGase F (P0704S, New

472 England Biolabs) and Endo-Hf (P0703L, New England Biolabs) were used according to the

473 manufacturer's instructions to treat RBC ghost samples prior to electrophoresis.

474 *Lectin precipitation*

475 RBC ghosts were suspended in equal volumes of calcium binding buffer containing 2% Triton

476 X-100, pre-cleared with magnetic streptavidin beads (88816, Pierce) and incubated with

477 biotinylated GNA lectin (1 mg/ml; B1245, Vector Laboratories), biotinylated MAL-II lectin (1

478 mg/ml; B1265, Vector Laboratories) or buffer only overnight at 4°C. Precipitation with magnetic

479 streptavidin beads was performed in binding buffer and the beads washed with binding buffer

480 containing 0.1% Triton X-100. Washed precipitates were denatured at 100°C for 10 minutes and

481 supernatants loaded for gel electrophoresis and blotting. Blots were probed with anti-spectrin

482 antibody (1 in 20,000 dilution; S3396, Sigma-Aldrich) and anti-mouse-HRP secondary antibody

483   (1 in 10,000 dilution, 5887, Abcam). PBS/0.1% Tween 20 replaced calcium binding buffer for

484   lectin blotting.

485   *Spectrin purification*

486   Spectrin was purified following the method of Ungewickell *et al*. with slight modifications (48).

487   Briefly, the ghosts were washed twice and resuspended in 3 volumes of 37°C pre-warmed

488   sodium phosphate (0.3 mM, pH 7.2) (extraction buffer) and incubated for 20 min at 37°C. The

489   fragmented ghosts were pelleted by centrifugation at 40000g for 1 hour at 2°C. Supernatant was

490   used as spectrin preparation for analysis.

491   *Serial trypsin dilution treatment of spectrin*

492   Spectrin preparations or ghosts were analysed for protein content by BCA assay. Titrations of

493   trypsin at concentrations as a fraction of sample concentration were applied for one hour or

494   longer if indicated, at 37°C. No trypsin addition was applied to the untreated sample, which was

495   also incubated for the same duration. Samples were all heat inactivated at 100°C for 10 minutes,

496   after diluting with 8M urea sample buffer at a 1:1 ratio.

497   *Chymotrypsin and pepsin digestions*

498   Chymotrypsin and pepsin were applied at 1:5 dilution in sample. Combinatorial protease

499   treatment over 48 hours were performed with heat inactivation for 100°C, 10 minutes at 24

500   hours. During pepsin treatment, sample was pre-diluted 1:1 with HCl, pH2.0. Acid was

501   neutralized with NaOH after 24 hours, prior to addition of other proteases.

502   *Isolation of trypsin resistant sickle fragment (TRSF)(F40)*

503   Approximately 20ml of HbSS ghosts, having been washed with low cold salt extraction buffer

504   (0.3M sodium phosphate, pH 7.6), was treated with 1:5 trypsin: sample ratio overnight. Heat

505   inactivation at 100°C was carried out for 10 minutes. Supernatant was harvested and further

506   centrifuged to remove insoluble products. Clarified supernatant was subsequently concentrated

507   with a 100kDa cut-off concentrator (Pierce, Thermo Fisher, 88533) and supernatant applied to

508   and concentrated with a 10kDa cut-off concentrator to approximately 500µl.

509   *Mass spectrometry glycomic analysis of TRSF*

510   Urea containing sample buffer, as above, was applied to TRSF. Coomassie bands corresponding

511   to 40-44kD region were cut and analysed in three segments: 39-40kD, 41-42kD and 43-44kD.

512   *Dual colour western*

513   Amersham western blotting machines was used to detect GNA lectin and anti-spectrin binding

514   using Cy3 and Cy5 conjugated reagents. Data were acquired and analysed by Amersham's

515   inbuilt software.

516   *Immunofluorescence microscopy*

517   Cell surface GNA lectin binding for immunofluorescence was performed as for flow cytometry

518   with minor alterations (10^7 cells per test, 8 µg/ml GNA lectin, 1 µg/ml Streptavidin PE. For Fig.

519   1b and Extended Data Fig.1c and 1d, 8 µg/ml GNA lectin and 1 µg/ml Streptavidin PE were pre-

520   complexed overnight). Intracellular GNA lectin binding followed fixation (0.005%

521   glutaraldehyde/PBS, 10 minutes, room temperature) and permeabilization (0.1% Triton-X

522   100/PBS, 15 minutes, room temperature). Stained cells were pulse centrifuged ($\leq$300g) for 30

523   seconds (including acceleration), in 24 well, flat bottom tissue culture plates (Greiner). To stain

524   CD206, cells were blocked for 15 minutes with 1% BSA/PBS at room temperature in the dark

525   and incubated with Alexa-488 conjugated anti-mannose receptor antibody (1.25 µg/ml, Clone

526   19.2; 53-2069-47, eBiosciences). DAPI (as per manufacturer's instructions; D1306, Thermo

527   Fisher) staining was applied to cells post fixation/permeabilization for 30 minutes at room

528   temperature. Cells were washed in PBS and imaged at 32x magnification using an

529   immunofluorescence microscope (Zeiss AxioObserver Z1). Images were analysed by Zen (Black

530   and Blue versions, Zeiss).

531   *siRNA knockdown of mannose receptor*

532   Human mannose receptor (CD206) siRNA (UACUGUCGCAGGUAUCAUCCA) or a non-

533   targeting siRNA sequence control (4390843, Life Technologies) were transfected into HMDM

534   (RNAiMax, Life Technologies) (n = 4 donors for all siRNA experiments). Knockdown

535   efficiency was established by determining mannose receptor expression by microscopy using

536   CD206-Alexa-488 staining (described above) in the small non-granular macrophage sub-

537   population by merging bright field and mannose receptor fluorescence staining. Knockdown

538   efficiency was typically 65-85% (Extended Data Fig. 6c).

539   *Confocal microscopy for RBCs*

540   For spectrin-GNA lectin double staining experiments, permeabilized RBCs were stained with

541   anti-human spectrin antibody (1 in 50 dilution; S3396, Sigma Aldrich) concurrently with GNA

542   lectin (8 µg/ml) in calcium buffer. Alexa Fluor 647 anti-mouse antibody (10 µg/ml; A31571,

543   Thermo Fisher) was applied in conjunction with streptavidin PE (1 µg/ml; Beckman Dickinson)

544   following staining of primary reagents. RBCs were gravity sedimented (30 minutes at room

545   temperature, in the dark) onto poly-L-lysine (Sigma Aldrich) treated 8 well chamber slides

546   (LabTek). Images were acquired by a Zeiss LSM 710 microscope.

547   *3D-Structured Illumination Microscopy (3DSIM)*

548   GNA lectin/anti-spectrin stained RBCs were gravity sedimented onto poly-L-lysine treated

549   chamber slides (LabTek). 3DSIM images were acquired on a N-SIM (Nikon Instruments, UK)

550   using a 100x 1.49NA lens and refractive index matched immersion oil (Nikon Instruments).

551   Samples were imaged using a Nikon Plan Apo TIRF objective (NA 1.49, oil immersion) and an

552   Andor DU-897X-5254 camera using 561 and 640nm laser lines. Z-step size for Z stacks was set

553   to 0.120 µm, as required by the manufacturer's software. For each focal plane, 15 images (5

554   phases, 3 angles) were captured with the NIS-Elements software. SIM image processing,

555   reconstruction and analysis were carried out using the N-SIM module of the NIS-Element

556   Advanced Research software. Images were checked for artefacts using SIMcheck software

557   (http://www.micron.ox.ac.uk/software/SIMCheck.php). Images were reconstructed using NiS

558   Elements software v4.6 (Nikon Instruments, Japan) from a Z stack comprising $\geq$1µm of optical

559   sections. In all SIM image reconstructions, the Wiener and Apodization filter parameters were

560   kept constant. Reconstructed SIM images were rendered in 3 dimensions using Imaris (Bitplane).

561   Intracellular GNA lectin and anti-spectrin staining of healthy RBCs was performed following

562   fixation and permeabilization. In order to co-localize surface GNA lectin with intracellular

563   spectrin, SCD RBCs were stained with GNA lectin/streptavidin-PE staining before, and anti-

564   spectrin/donkey anti-mouse Alexa 647 after, fixation and permeabilization.

565

566   *P. falciparum culture in RBCs of different genotypes and flow cytometry analysis*

567   *P. falciparum* IT/FCR3 parasites were cultured at 2% haematocrit in supplemented RPMI as

568   described (49). Mature trophozoite-infected erythrocytes were purified to >90% parasitaemia by

569   magnetic separation with a MACS CS column (Miltenyi Biotec, Germany) (50). The purified

570   infected erythrocytes were used to infect RBCs of different genotypes with a starting

571   parasitaemia of approximately 0.5%. RBCs were used within 10 days post-bleed, typically 3-5

572   days. Cultures were gassed with 1% oxygen, 3% carbon dioxide and 96% nitrogen, then

573   incubated at 37°C for 48-72 hours. After one cycle of invasion and growth, flow cytometry was

574   used to assess parasitaemia and parasite maturation (51), as well as GNA lectin -binding and

575   PfEMP1 antibody staining. This method uses internally controlled flow cytometry analysis to

576   separate uninfected red cells, ring-stage, trophozoite and schizont stage parasites within the same

577   culture by FACS gating, using a pair of DNA- and RNA-binding dyes (Extended Data Fig. 9b,

578   c). Hypoxia-induced reduction in parasite invasion and growth was observed in HbAS red cells,

579   as described by Archer *et al.* (8). However, a range of parasite stages was available within each

580   culture to allow investigation of high mannose exposure as parasites matured through the blood

581   stage cycle.

582   For flow cytometry, infected erythrocytes in binding buffer (10mM HEPES, 150mM NaCl,

583   2.5mM $CaCl_2$, pH 7.4) were stained with Vybrant Violet (Thermo Fisher, V35003, 2.5μM) and

584   ethidium bromide (Sigma-Aldrich, 46067-50ml-F, 1% in dH_20). Biotinylated GNA lectin

585   staining was performed as described above. Streptavidin APC was used to detect biotinylated

586   GNA lectin. A BD LSRFortessa (BD Biosciences) was used for flow cytometry and

587   compensation between channels was carried out prior to the experiment. Relative GNA lectin

588   binding was calculated for ring, trophozoite and schizont gates by dividing the gMFI for each

589   gate by the value measured in the uninfected RBC gate. PfEMP1 expression was assessed using

590   a rabbit polyclonal antibody raised against the N-terminal region (DBLαCIDR didomain) of the

591   predominant PfEMP1 variant expressed in the culture (ITvar70, also known as AFBR6) (52), as

592   described previously (53). The staining with PfEMP1 antibody (purified total IgG at 10 μg/ml for

593   30 mins, followed by APC-conjugated goat anti-rabbit Alexa 647 (Invitrogen, A21244, 2 μg/ml))

594   was compared to rabbit IgG control antibody (10 μg/ml, total IgG from a non-immunized rabbit,

595   followed by secondary antibody as above). Normalized PfEMP1 gMFI was calculated by

596   subtracting gMFI for rabbit IgG control antibody staining from that of the PfEMP1 antibody

597   staining. Relative PfEMP1 expression for all samples is expressed as a percentage of the average

28

598   HbAA schizont PfeMP1 expression per experiment, which typically contained three HbAA

599   samples.

600   *Statistical analysis*

601   Most data are treated as non-parametrically distributed and presented with medians and

602   interquartile ranges, with the exception of Fig. 5c, where means and standard deviations are

603   shown. Statistical significance was assessed by either two-tailed Mann-Whitney (non-paired

604   data) or two-tailed Wilcoxon signed rank tests (paired data). Multiple comparisons between

605   stages of RBC infection by *P. falciparum* were analysed by ANOVA. All calculations were

606   implemented in Prism version 5.04 (GraphPad Software).

607

608   **Data Availability**

609   The authors declare that the data supporting the findings of this study are available within the

610   paper and its supplementary information files. Further data are available from the corresponding

611   author upon reasonable request.

612

613   References

614   1. Piel FB, Steinberg MH, Rees DC. Sickle Cell Disease. N Engl J Med. 2017 April
615   20;376(16):1561-73.

616   2. Rees DC, Williams TN, Gladwin MT. Sickle-cell disease. Lancet. 2010 December
617   11;376(9757):2018-31.

618   3. Brousse V, Buffet P, Rees D. The spleen and sickle cell disease: the sick(led) spleen. Br J
619   Haematol. 2014 July 01;166(2):165-76.

620   4. Hebbel RP, Miller WJ. Phagocytosis of sickle erythrocytes: immunologic and oxidative
621   determinants of hemolytic anemia. Blood. 1984 September 01;64(3):733-41.

622   5. ALLISON AC. Protection afforded by sickle-cell trait against subtertian malareal infection. Br
623   Med J. 1954 February 06;1(4857):290-4.

624   6. Luzzatto L. Sickle cell anaemia and malaria. Mediterr J Hematol Infect Dis.
625   2012;4(1):e2012065.

626   7. Ayi K, Turrini F, Piga A, Arese P. Enhanced phagocytosis of ring-parasitized mutant
627   erythrocytes: a common mechanism that may explain protection against falciparum malaria in
628   sickle trait and beta-thalassemia trait. Blood. 2004 November 15;104(10):3364-71.

629   8. Archer NM, Petersen N, Clark MA, Buckee CO, Childs LM, Duraisingh MT. Resistance to
630   Plasmodium falciparum in sickle cell trait erythrocytes is driven by oxygen-dependent growth
631   inhibition. Proc Natl Acad Sci U S A. 2018 July 10;115(28):7350-5.

632   9. Brown GD, Crocker PR. Lectin Receptors Expressed on Myeloid Cells. Microbiol Spectr.
633   2016 October 01;4(5):10.1128/microbiolspec.MCHD-0036.

634   10. Shibuya N, Goldstein IJ, Van Damme EJ, Peumans WJ. Binding properties of a mannose-
635   specific lectin from the snowdrop (Galanthus nivalis) bulb. J Biol Chem. 1988 January
636   15;263(2):728-34.

637   11. Kaku H, Van Damme EJ, Peumans WJ, Goldstein IJ. Carbohydrate-binding specificity of the
638   daffodil (Narcissus pseudonarcissus) and amaryllis (Hippeastrum hybr.) bulb lectins. Arch
639   Biochem Biophys. 1990 June 01;279(2):298-304.

640   12. Erwig LP, Gow NA. Interactions of fungal pathogens with phagocytes. Nat Rev Microbiol.
641   2016 March 01;14(3):163-76.

642   13. Weatherall, D J & Clegg. The Thalassaemia Syndromes
643   . 4th ed. Blackwell Science Ltd; 2008.

644   14. Kato GJ, Steinberg MH, Gladwin MT. Intravascular hemolysis and the pathophysiology of
645   sickle cell disease. J Clin Invest. 2017 March 01;127(3):750-60.

646   15. Chirico EN, Pialoux V. Role of oxidative stress in the pathogenesis of sickle cell disease.
647   IUBMB Life. 2012 January 01;64(1):72-80.

648   16. Niihara Y, Miller ST, Kanter J, Lanzkron S, Smith WR, Hsu LL, et al. A Phase 3 Trial of l-
649   Glutamine in Sickle Cell Disease. N Engl J Med. 2018 July 19;379(3):226-35.

650   17. Linehan SA, Martinez-Pomares L, da Silva RP, Gordon S. Endogenous ligands of
651   carbohydrate recognition domains of the mannose receptor in murine macrophages, endothelial
652   cells and secretory cells; potential relevance to inflammation and immunity. Eur J Immunol.
653   2001 June 01;31(6):1857-66.

654   18. Martinez-Pomares L. The mannose receptor. J Leukoc Biol. 2012 December 01;92(6):1177-
655   86.

656   19. Wagener J, Malireddi RK, Lenardon MD, Koberle M, Vautier S, MacCallum DM, et al.
657   Fungal chitin dampens inflammation through IL-10 induction mediated by NOD2 and TLR9
658   activation. PLoS Pathog. 2014 April 10;10(4):e1004050.

659   20. D'Amici GM, Rinalducci S, Zolla L. Proteomic analysis of RBC membrane protein
660   degradation during blood storage. J Proteome Res. 2007 August 01;6(8):3242-55.

661   21. Murphy SC, Samuel BU, Harrison T, Speicher KD, Speicher DW, Reid ME, et al.
662   Erythrocyte detergent-resistant membrane proteins: their characterization and selective uptake
663   during malarial infection. Blood. 2004 March 01;103(5):1920-8.

664   22. Percario S, Moreira DR, Gomes BA, Ferreira ME, Goncalves AC, Laurindo PS, et al.
665   Oxidative stress in malaria. Int J Mol Sci. 2012 December 03;13(12):16346-72.

666   23. Del Portillo HA, Ferrer M, Brugat T, Martin-Jaular L, Langhorne J, Lacerda MV. The role of
667   the spleen in malaria. Cell Microbiol. 2012 March 01;14(3):343-55.

668   24. Safeukui I, Correas JM, Brousse V, Hirt D, Deplaine G, Mule S, et al. Retention of
669   Plasmodium falciparum ring-infected erythrocytes in the slow, open microcirculation of the
670   human spleen. Blood. 2008 September 15;112(6):2520-8.

671   25. Wahlgren M, Goel S, Akhouri RR. Variant surface antigens of Plasmodium falciparum and
672   their roles in severe malaria. Nat Rev Microbiol. 2017 August 01;15(8):479-91.

673   26. Cholera R, Brittain NJ, Gillrie MR, Lopera-Mesa TM, Diakite SA, Arie T, et al. Impaired
674   cytoadherence of Plasmodium falciparum-infected erythrocytes containing sickle hemoglobin.
675   Proc Natl Acad Sci U S A. 2008 January 22;105(3):991-6.

676   27. Opi DH, Uyoga S, Orori EN, Williams TN, Rowe JA. Red blood cell complement receptor
677   one level varies with Knops blood group, alpha(+)thalassaemia and age among Kenyan children.
678   Genes Immun. 2016 April 01;17(3):171-8.

679   28. Martinez-Pomares L, Hanitsch LG, Stillion R, Keshav S, Gordon S. Expression of mannose
680   receptor and ligands for its cysteine-rich domain in venous sinuses of human spleen. Lab Invest.
681   2005 October 01;85(10):1238-49.

682   29. Cyrklaff M, Sanchez CP, Kilian N, Bisseye C, Simpore J, Frischknecht F, et al. Hemoglobins
683   S and C interfere with actin remodeling in Plasmodium falciparum-infected erythrocytes.
684   Science. 2011 December 02;334(6060):1283-6.

685   30. Cyrklaff M, Srismith S, Nyboer B, Burda K, Hoffmann A, Lasitschka F, et al. Oxidative
686   insult can induce malaria-protective trait of sickle and fetal erythrocytes. Nat Commun. 2016
687   November 08;7:13401.

688   31. Zamze S, Martinez-Pomares L, Jones H, Taylor PR, Stillion RJ, Gordon S, et al. Recognition
689   of bacterial capsular polysaccharides and lipopolysaccharides by the macrophage mannose
690   receptor. J Biol Chem. 2002 November 01;277(44):41613-23.

691   32. Li W. Eat-me signals: keys to molecular phagocyte biology and "appetite" control. J Cell
692   Physiol. 2012 April 01;227(4):1291-7.

693   33. Davies MJ. Protein oxidation and peroxidation. Biochem J. 2016 April 01;473(7):805-25.

694   34. Fibach E, Rachmilewitz E. The role of oxidative stress in hemolytic anemia. Curr Mol Med.
695   2008 November 01;8(7):609-19.

696   35. Kriebardis AG, Antonelou MH, Stamoulis KE, Economou-Petersen E, Margaritis LH,
697   Papassideri IS. Progressive oxidation of cytoskeletal proteins and accumulation of denatured
698   hemoglobin in stored red cells. J Cell Mol Med. 2007 February 01;11(1):148-55.

699   36. Snyder LM, Leb L, Piotrowski J, Sauberman N, Liu SC, Fortier NL. Irreversible spectrin-
700   haemoglobin crosslinking in vivo: a marker for red cell senescence. Br J Haematol. 1983 March
701   01;53(3):379-84.

702   37. Snyder LM, Fortier NL, Trainor J, Jacobs J, Leb L, Lubin B, et al. Effect of hydrogen
703   peroxide exposure on normal human erythrocyte deformability, morphology, surface
704   characteristics, and spectrin-hemoglobin cross-linking. J Clin Invest. 1985 November
705   01;76(5):1971-7.

706   38. Nur E, Biemond BJ, Otten HM, Brandjes DP, Schnog JJ, CURAMA Study Group. Oxidative
707   stress in sickle cell disease; pathophysiology and potential implications for disease management.
708   Am J Hematol. 2011 June 01;86(6):484-9.

709   39. Reisz JA, Wither MJ, Dzieciatkowska M, Nemkov T, Issaian A, Yoshida T, et al. Oxidative
710   modifications of glyceraldehyde 3-phosphate dehydrogenase regulate metabolic reprogramming
711   of stored red blood cells. Blood. 2016 September 22;128(12):e32-42.

712   40. Manno S, Mohandas N, Takakuwa Y. ATP-dependent mechanism protects spectrin against
713   glycation in human erythrocytes. J Biol Chem. 2010 October 29;285(44):33923-9.

714   41. Sinha A, Chu TT, Dao M, Chandramohanadas R. Single-cell evaluation of red blood cell bio-
715   mechanical and nano-structural alterations upon chemically induced oxidative stress. Sci Rep.
716   2015 May 07;5:9768.

717   42. Aoki T. A Comprehensive Review of Our Current Understanding of Red Blood Cell (RBC)
718   Glycoproteins. Membranes (Basel). 2017 September 29;7(4):10.3390/membranes7040056.

719   43. Hoppe CA, Lee YC. The binding and processing of mannose-bovine serum albumin
720   derivatives by rabbit alveolar macrophages. Effect of the sugar density. J Biol Chem. 1983
721   December 10;258(23):14193-9.

722   44. McGreal EP, Rosas M, Brown GD, Zamze S, Wong SY, Gordon S, et al. The carbohydrate-
723   recognition domain of Dectin-2 is a C-type lectin with specificity for high mannose.
724   Glycobiology. 2006 May 01;16(5):422-30.

725   45. Barker RN, Casswell KM, Reid ME, Sokol RJ, Elson CJ. Identification of autoantigens in
726   autoimmune haemolytic anaemia by a non-radioisotope immunoprecipitation method. Br J
727   Haematol. 1992 September 01;82(1):126-32.

728   46. Jang-Lee J, North SJ, Sutton-Smith M, Goldberg D, Panico M, Morris H, et al. Glycomic
729   profiling of cells and tissues by mass spectrometry: fingerprinting and sequencing
730   methodologies. Methods Enzymol. 2006;415:59-86.

731   47. Ceroni A, Maass K, Geyer H, Geyer R, Dell A, Haslam SM. GlycoWorkbench: a tool for the
732   computer-assisted annotation of mass spectra of glycans. J Proteome Res. 2008 April
733   01;7(4):1650-9.

734   48. Ungewickell E, Gratzer W. Self-association of human spectrin. A thermodynamic and kinetic
735   study. Eur J Biochem. 1978 August 01;88(2):379-85.

736   49. Corrigan RA, Rowe JA. Strain variation in early innate cytokine induction by Plasmodium
737   falciparum. Parasite Immunol. 2010 July 01;32(7):512-27.

738   50. Staalsoe T, Giha HA, Dodoo D, Theander TG, Hviid L. Detection of antibodies to variant
739   antigens on Plasmodium falciparum-infected erythrocytes by flow cytometry. Cytometry. 1999
740   April 01;35(4):329-36.

741   51. Ch'ng JH, Moll K, Quintana Mdel P, Chan SC, Masters E, Moles E, et al. Rosette-Disrupting
742   Effect of an Anti-Plasmodial Compound for the Potential Treatment of Plasmodium falciparum
743   Malaria Complications. Sci Rep. 2016 July 11;6:29317.

744   52. Viebig NK, Levin E, Dechavanne S, Rogerson SJ, Gysin J, Smith JD, et al. Disruption of
745   var2csa gene impairs placental malaria associated adhesion phenotype. PLoS One. 2007
746   September 19;2(9):e910.

747   53. Ghumra A, Khunrae P, Ataide R, Raza A, Rogerson SJ, Higgins MK, et al. Immunisation
748   with recombinant PfEMP1 domains elicits functional rosette-inhibiting and phagocytosis-
749   inducing antibodies to Plasmodium falciparum. PLoS One. 2011 January 31;6(1):e16414.

750

751

752 **Supplemental Information**

753 Extended Data Tables 1-3.

754 Extended Data Figs. 1-9.

755 Extended Data File 1.

756

757 **Acknowledgements**

771

772 **Author contributions**

773 H.C. carried out experiments, analysed data and wrote the paper. S.H., A.M., B.P., J.S., H.W.,

774 M.A.F., E.B., S.L., G.K., B.M., M-L.W., A. Davie, D.T., M.M., L.H., C.L., W.P. carried out

775 experiments. J.B., supervised by D.C.R., and B.R. obtained blood samples. A.A. obtained and

776 analysed glycomic and proteomic data, supervised by S.M.H. and A. Dell. L.E., G.D.B. and

777 H.M.W. helped supervise the project. J.A.R. carried out experiments, analysed data and wrote

778 the paper. R.N.B. and M.A.V. conceived and supervised the project, and wrote the paper.

779

780 **Author information**

781 The authors declare the existence of a financial competing interest. The University of Aberdeen

782 has applied for patents covering diagnostic and therapeutic applications arising from the work

783 described in this paper. Correspondence and requests for materials should be addressed to

784 M.A.V. (m.a.vickers@abdn.ac.uk) or A.R. (Alex.Rowe@ed.ac.uk).

785

786 **Data Availability**

787 Some source data are provided in the online version of the paper. The other datasets generated

788 during and/or analysed during the current study are available from the corresponding authors on
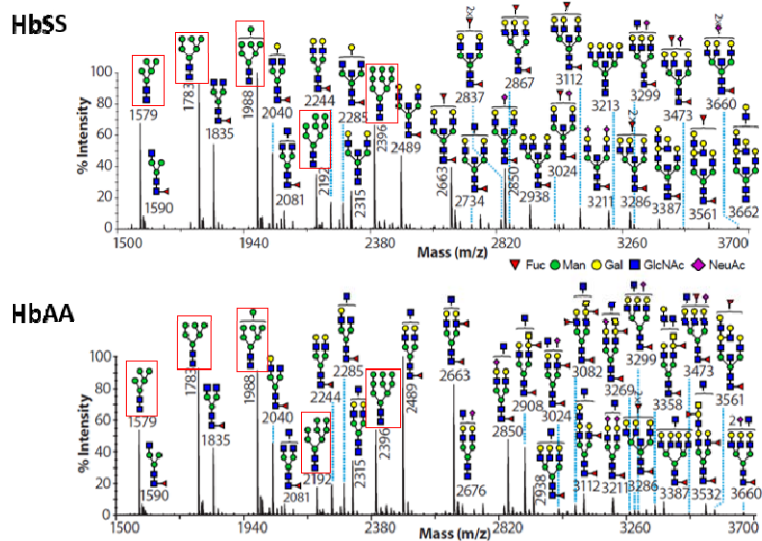
789 reasonable request.

Figure 1
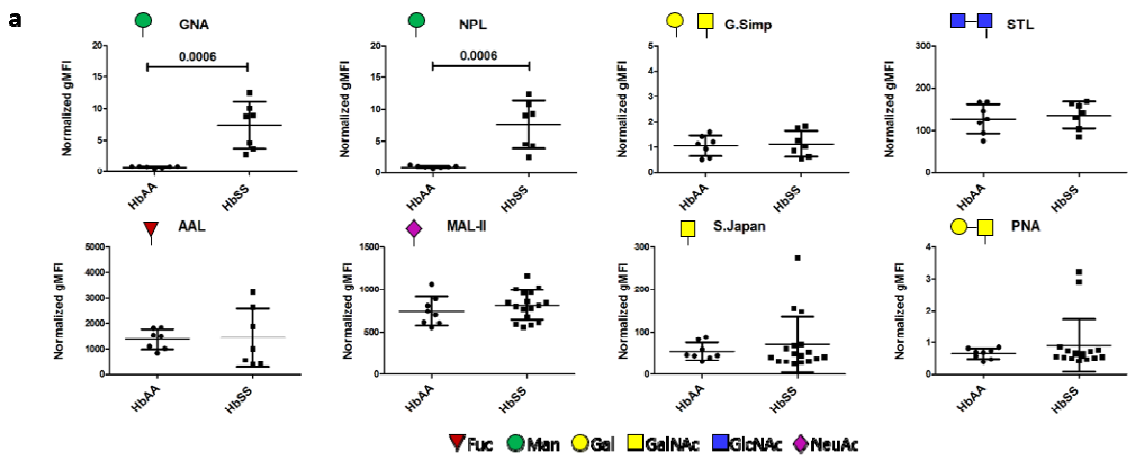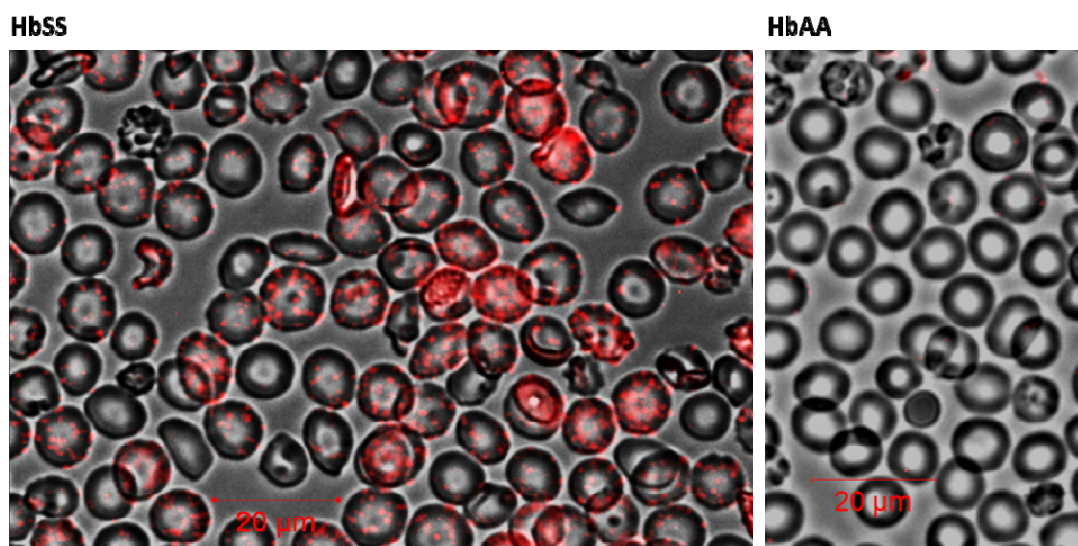
791   **Figure 1: HbSS RBCs are characterized by microdomain expression of surface mannoses.**

792   a) Whole blood flow cytometry analysis of HbAA and HbSS RBCs using fluorescently

793   labelled plant lectins, detailed in Methods. Vertical axes show normalized geometric

794   mean fluorescence (gMFI). Symbols of terminal carbohydrate detected by plant lectins

795   are indicated. Data shown as median +/- IQR, n=7 per group for significant differences, 2

796   tailed Mann-Whitney p values shown, distinct samples measured once each, 3 separate

797   experiments. Annotation uses conventional symbols for carbohydrates in accordance with

798   http://www.functionalglycomics.org guidelines: purple diamond, sialic acids; yellow

799   circle, galactose; blue square, N-acetyl glucosamine; green circle, mannose; red triangle,

800   fucose.

801   b) GNA lectin staining (red) of HbSS and HbAA RBCs, immunofluorescence, merged with

802   bright field.

803   c) MALDI-ToF mass spectra (m/z versus relative intensity) for glycomic analysis of N-

804   glycans from membrane ghosts from individual HbSS and HbAA donors. Red boxes

805   indicate high mannose structures. Annotation uses conventional symbols for

806   carbohydrates in accordance with http://www.functionalglycomics.org guidelines: purple

807   diamond, sialic acids; yellow circle, galactose; blue square, N-acetyl glucosamine; green

808   circle, mannose; red triangle, fucose. Only major structures are annotated for clarity. Full

809   spectra of both HbSS and HbAA donors are shown in Extended Data Fig. 9.

810

811

Figure 2
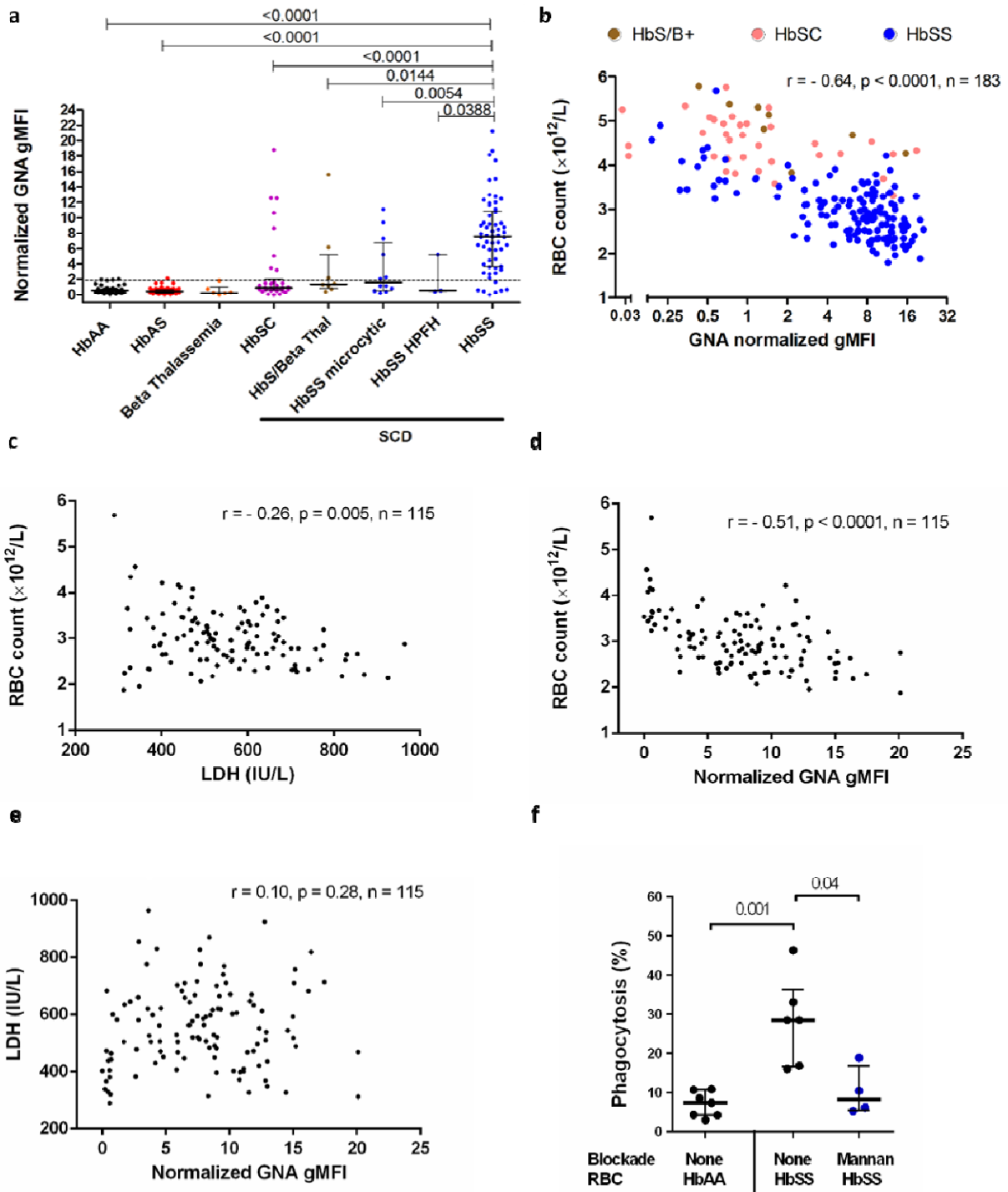
812

813

814   **Figure 2: Mannose expression correlate to clinical anaemia in SCD**

815   a) Normalized gMFI of GNA lectin staining of RBCs from peripheral blood samples,

816   comparing RBC from patients with sub-types of SCD (milder phenotypes: HbSC (n=34),

817   HbS/beta-thal (n=8), HbSS microcytic (n=12) and HbSS HPFH (n=3) indicate compound

818   heterozygosity for HbC, β-thalassaemia, α-thalassaemia and hereditary persistence of

819   fetal haemoglobin respectively) versus healthy donors (n=45), sickle cell trait (n=57) and

820   β-thalassaemia (n=6). Dotted line indicates 90th centile of GNA lectin binding within

821   healthy samples. Data shown as median +/- IQR, 2 tailed Mann-Whitney p values shown,

822   distinct samples measured once each, numerous experiments.

823   b) Plot of RBC count against normalized GNA gMFI for SCD: HbS/B+ and HbSC indicates

824   compound heterozygosity for HbS with β-thalassaemia and HbC respectively;

825   Spearman's rank correlation.

826   Plots of:

827   c) RBC count versus serum lactate dehydrogenase (LDH),

828   d) RBC count vs GNA binding,

829   e) LDH vs GNA lectin binding; HbSS RBCs for which corresponding serum LDH values

830   were available; Spearman's rank correlation,

831   f) Percentage phagocytosis of HbAA and HbSS RBCs by human monocyte derived

832   macrophages analysed by microscopy. Mannan inhibition as shown. Each data point

833   represents a different RBC donor. Mann-Whitney; pooled from two experiments.
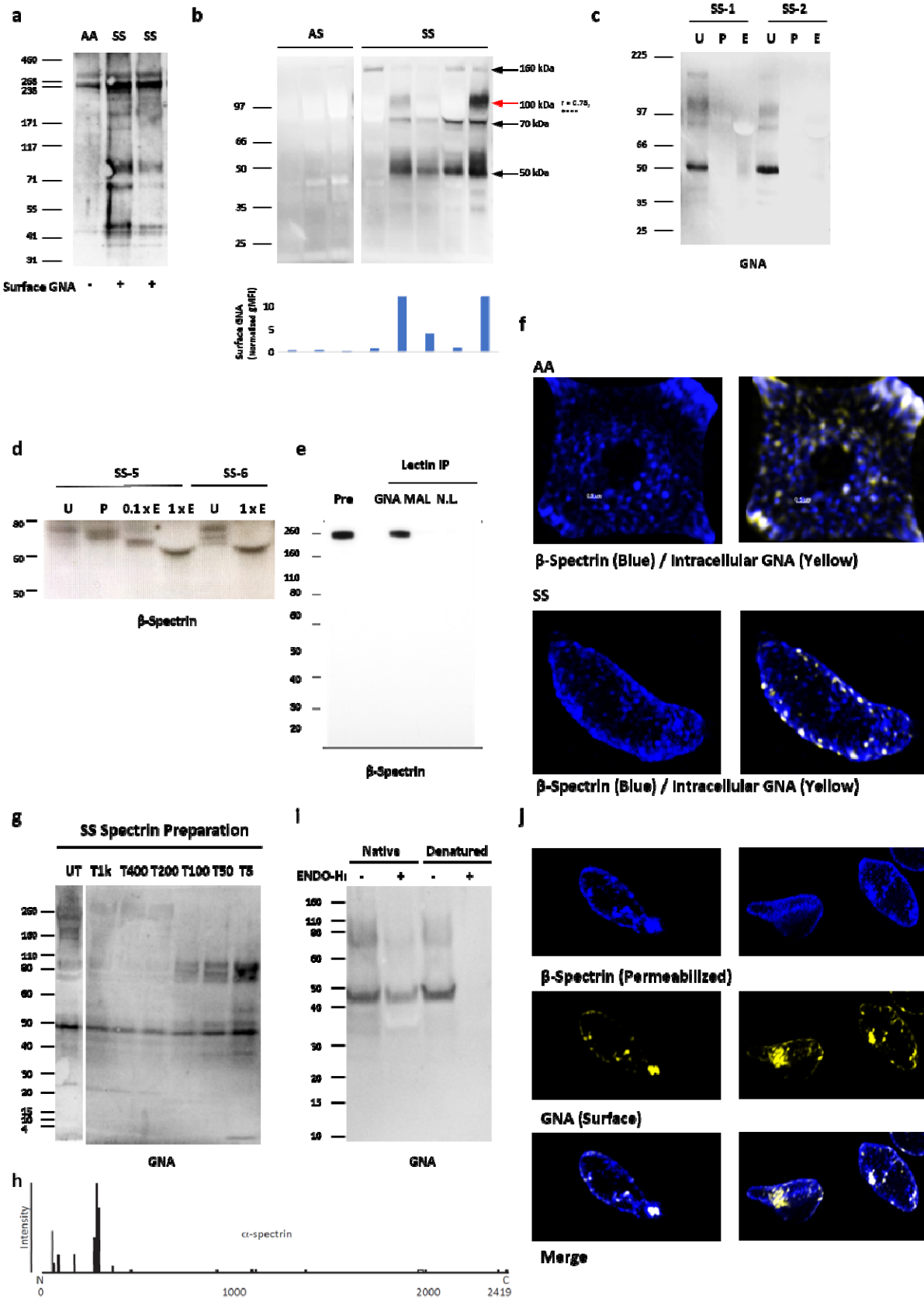
834

Figure 3
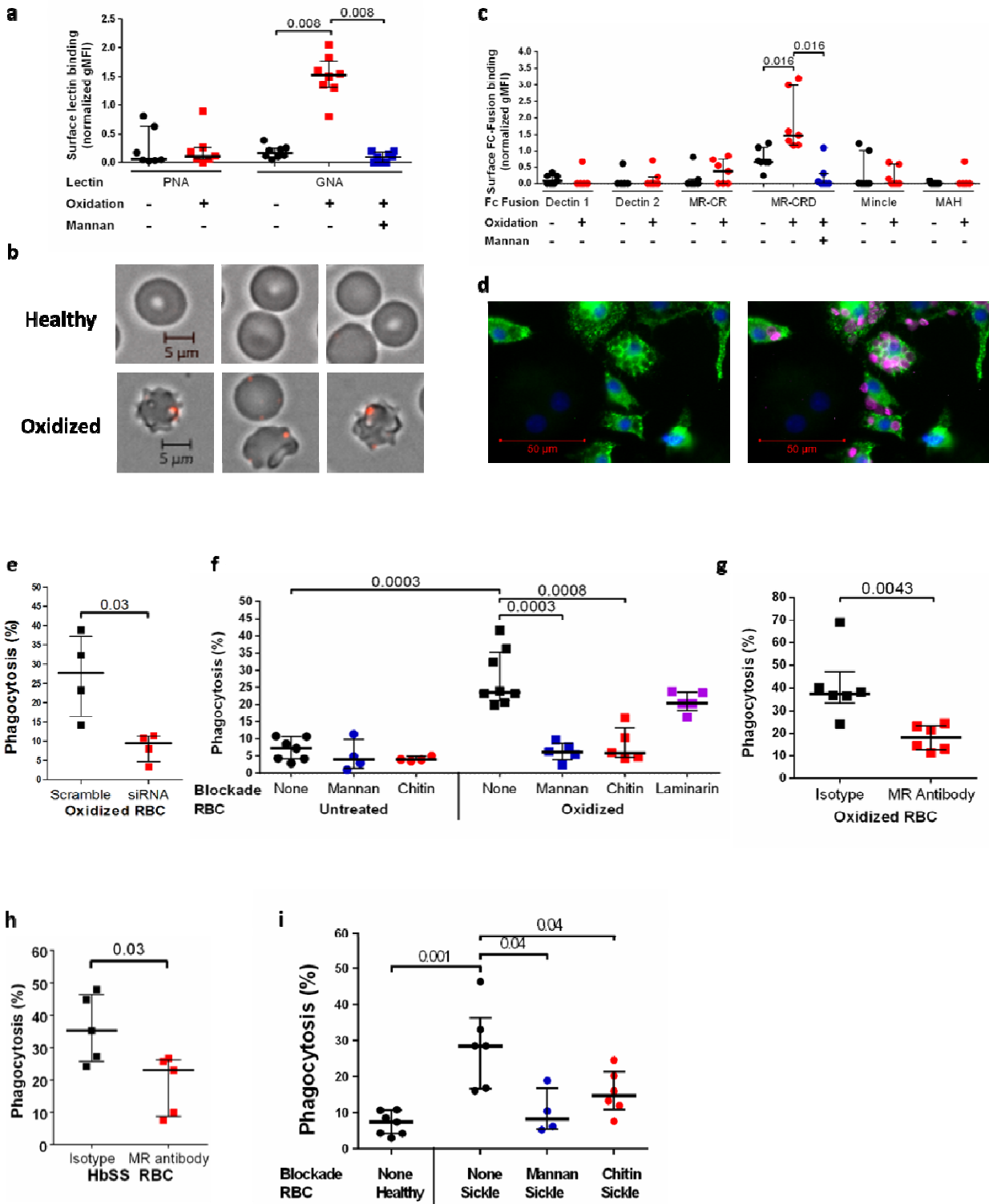
835
836 **Figure 3: Display of membrane skeleton associated mannose patches is induced by**

837 **oxidative stress and recognized by the mannose receptor on macrophages.**

838 a) PNA and GNA lectin binding to HbAA RBCs with or without oxidation. Mannan

839 blockade for GNA lectin binding shown in blue. Wilcoxon, paired data, pooled from two

840 independent experiments.

841 b) Immunofluorescence microscopy of GNA lectin/streptavidin (red) staining of healthy

842 HbAA RBCs (above) and after oxidative insult (below).

843 c) Normalized gMFI for binding analysed by flow cytometry of murine Fc fusions with C-

844 type lectins or sub-domains applied to oxidized versus undamaged RBCs. Mannan

845 blockade of MR-CRD binding is shown in blue. MAH, macrophage antigen H. CR,

846 cysteine rich. CRD, carbohydrate recognition domain. Wilcoxon, paired data, pooled

847 from two independent experiments.

848 d) Immunofluorescence microscopy image of human monocyte derived macrophages

849 (HMDM) stained with DAPI (blue) and for mannose receptor (green) after incubation

850 with oxidized HbAA RBCs, shown in magenta.

851 e) Percentage phagocytosis of oxidized RBCs by HMDM treated with human MR specific

852 or scrambled siRNA. Mann-Whitney, 2 experiments.

853 f) Percentage phagocytosis of healthy or oxidized HbAA RBCs by HMDM with or without

854 pre-blocking by mannan, chitin or laminarin

855 g) As (f) but oxidized RBCs are blocked by MR-CRD blocking antibody 15.2 as indicated.

856 Mann-Whitney.

857 h) Percentage phagocytosis of HbSS RBCs with or without pre-blocking by MR-CRD

858 blocking antibody 15.2. Mann-Whitney, 3 experiments.

859   i)   HbAA unblocked and HbSS unblocked or mannan and chitin blockade phagocytosis

860   experiments as shown.

Figure 4

β-Spectrin (Blue) / Intracellular GNA (Yellow)

β-Spectrin (Blue) / Intracellular GNA (Yellow)

β-Spectrin (Permeabilized)

GNA (Surface)

Merge

861

862   **Figure 4: High mannose decoration of spectrin containing fragments in sickle cell disease**

863   a)   GNA lectin western blot from healthy (HbAA) and sickle (HbSS) ghosts.

864   b)   Above are shown further GNA lectin western blots from HbAA and HBSS ghosts.

865   The histogram below the blot shows the flow cytometrically measured surface GNA

866   lectin staining values of the RBCs used to make the ghosts, with each bar

867   corresponding to the cells used to make the western lane above. The r value to the

868   right of the 100kDa size label is Spearman's rank correlation coefficient between

869   GNA lectin staining values and band intensities, both classified ordinally as high,

870   medium or low (n=27 measurements from 22 individuals). None of the other bands

871   yielded significant correlation coefficients.

872   c)   GNA lectin blot from HbSS ghosts: untreated (U), treated by PNGase (P) or Endo-H

873   (E).

874   d)   High exposure β-spectrin blot showing PNGase and partial/full (0.1X/1X) Endo-H

875   digestion of two HbSS ghosts.

876   e)   Lectin precipitation of healthy ghosts with GNA or MAL-II lectins. No lectin control

877   is also shown. Immunoblot with β-spectrin specific antibody.

878   f)   Super resolution microscopy image of spectrin membrane skeleton (blue) from

879   healthy (AA) and sickle cells (SS). Yellow clusters of GNA staining are overlaid. 3D

880   image is sliced to reveal single sheet of membrane skeleton network.

881   g)   GNA lectin blot of spectrin released from HbSS ghosts after digestion with trypsin

882   for one hour. Untreated (UT), Tx indicates the dilution factor of trypsin relative to

883   spectrin material.

45

884   h)   Peptide coverage and intensity map of α-spectrin from proteomic analysis of F40

885   following chymotrypsin treatment.

886   i)   GNA lectin blots showing Endo-H treatment of the 10kDa concentrate from (e) under

887   native or denaturing conditions (urea/SDS/2-mercaptoethanol) for 24 hours.

888   j)   3D SIM super-resolution microscopy of surface GNA lectin binding and internal β-

889   spectrin in HbSS. HbSS RBC are first stained with GNA lectin (yellow), then

890   permeabilized, and stained with anti-spectrin antibody (blue).

891

Figure 5

892
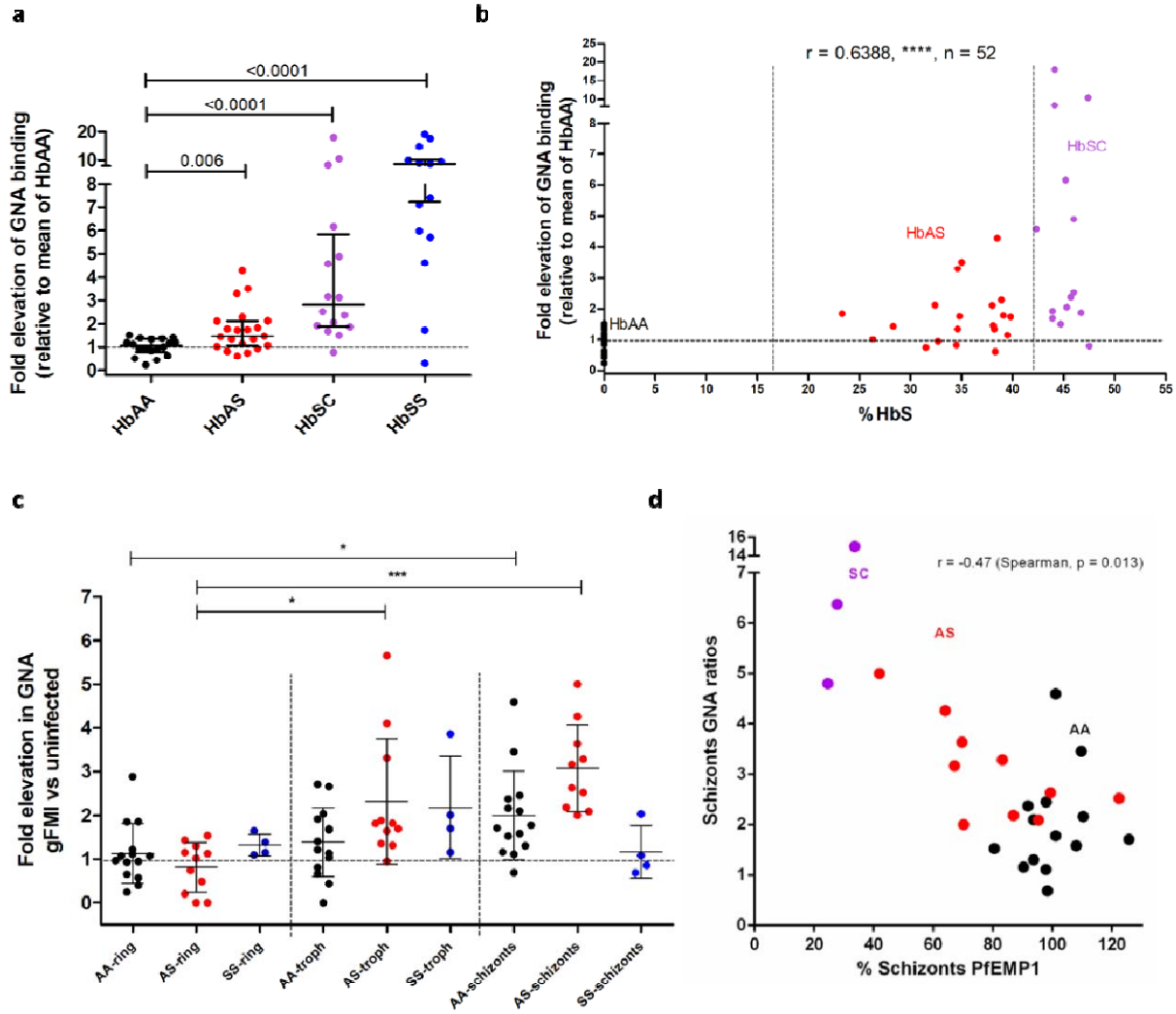
893 **Figure 5: High levels of mannose are displayed by sickle cell trait RBCs in response to both**

894 **oxidative stress and infection with *P. falciparum*.**

895 a) GNA lectin binding to HbAA versus HbAS, HbSC, HbSS RBCs in response to oxidative

896 stress, expressed as ratio to mean of oxidized HbAA samples. >5 experiments, Mann-

897 Whitney.

898 b) HbS percentage is plotted against elevation of GNA lectin binding in response to

899 oxidative stress as in (a). HbAA, HbAS and HbSC donor samples are shown as indicated.

900 Spearman's rank statistics shown.

901 c) GNA binding to HbAA, HbAS and HbSS RBCs in response to infection with *P.*

902 *falciparum*. Values for rings, trophozoites and schizonts are expressed as ratios relative to

903 the uninfected gate. Linked ANOVA analysis for HbAA (*, $p<.05$), HbAS (***, $p<.001$),

904 HbSS (n.s.); Tukey's multiple comparison within each genotype, 5 experiments.

905 d) Plot of relative GNA lectin binding for RBCs infected by schizonts against relative

906 PfEMP1 expression. Haemoglobin phenotypes of donors as indicated, Spearman's rank.

907

48

908 **Extended Data Table 1: Exclusion of possible lectin binding artefacts for SCD RBCs.**

909

Potential artefact	Exclusion
Non-specific binding of GNA lectin	• Wide lectin panel shows specificity (Fig.1a) • NPL lectin binding highly correlated with GNA lectin binding across all samples (Extended Data Fig. 1a) • Mannan blockade (Extended Data Fig. 1b) • No binding of GNA lectin to non-SCD haemolytic anaemia, HbAA and HbAS RBCs (Fig. 2a, Extended Data Fig. 2a)
Non-specific binding on sickle cells	Little binding with Annexin V (Extended Data Fig. 2b), in contrast to eryptotic RBC control (Extended Data Fig. 2c)
Sickle cells permeable to lectins	Lack of binding of other lectins or antibodies against intracellular antigens, BRIC-132/163 (Extended Data Fig. 4d)
O-GlcNAc detection instead of high mannose	No surface binding by antibody RL2, specific for O-GlcNAc (Extended Data Fig. 4e for oxidized RBCs and Extended Data Fig. 4f for HbSS RBCs)
Reticulocytosis	Lack of expression on non-SCD RBCs with high reticulocyte counts (Extended Data Fig. 3d, e).
Intravascular haemolysis	LDH independence (Fig. 2c, d, e)

910

911 **Extended Data Table 2**. Proteomic LC-MS analysis of 260kDa band cut from SDS-PAGE of

912 ghosts from healthy (HbAA) RBCs. Proteins included are with minimum: 99.5% probability, 3

913 peptides identified, and 5.0% sequence coverage. Common contaminants (e.g. keratins and

914 trypsin) have been removed. Identified proteins (UniProt accession, entry codes and description)

915 were sorted based on the number of sequence coverage (%Cov). MW, molecular weight in Da;

916 PLGS score, ProteinLynx Globar Server score.

917

918

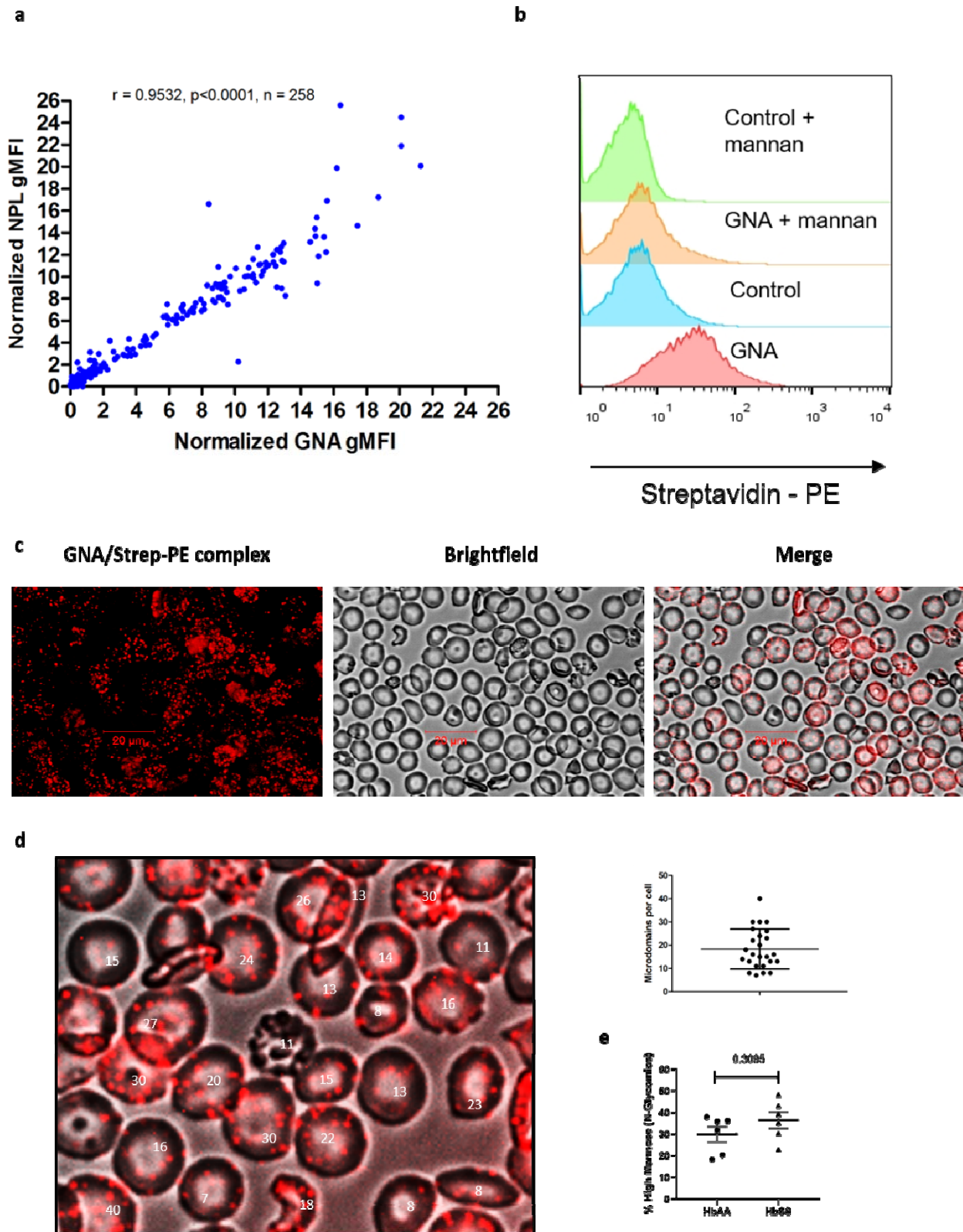| Accession	Entry	Description	MW	PLGS score	Prob. (%)	Peptides	%Cov
P02549	SPTA1_HUMAN	Spectrin alpha chain, erythrocytic 1 OS=Homo sapiens	279840	9.9	100.0	125	53.5
P11277	SPTB1_HUMAN	Spectrin beta chain, erythrocytic OS=Homo sapiens	246313	9.9	100.0	46	26.6
P02730	B3AT_HUMAN	Band 3 anion transport protein OS=Homo sapiens	101727	9.9	100.0	14	19.0
P16157	ANK1_HUMAN	Ankyrin-1 OS=Homo sapiens	206136	9.9	100.0	25	17.0
P11166	GTR1_HUMAN	Solute carrier family 2, facilitated glucose transporter member 1 OS=Homo sapiens	54048	9.9	100.0	3	6.3

919

50

920 **Extended Data Table 3**. Proteomic analysis of F40 trypsin resistant gel band identified α-
921 spectrin peptides (accession P02549, entry SPTA1_HUMAN), sorted on intensities. Peak MW,
922 molecular weight of the protonated (MH+) peptide found in Da; peptide MW, theoretical
923 molecular weight of the protonated (MH+) peptide in Da; delta, difference between peak MW
924 and peptide MW in ppm; score, PLGS score. In peptide sequence, cysteine (C) amino acids in
925 **bold** and underlined correspond to carboxymethylated cysteine amino acid.

926
927

Peak MW (MH+)	Peptide MW (MH+)	Delta (ppm)	Score	Sequence Start	End	Sequence	Intensity
1550.795	1550.795	0.08	6.8	280	292	IKEKEPVLTSEDY	317025
1135.598	1135.599	-1.18	6.6	293	303	GKDLVASEGLF	226142
643.359	643.356	4.36	6.3	54	58	HLQVF	146116
1245.657	1245.659	-1.14	6.1	270	279	KRDVTEAIQW	119871
1203.611	1203.612	-0.93	5.6	59	68	KRDADDLGKW	34163
1164.551	1164.553	-2.02	5.5	82	91	EDPTNIQGKY	63659
1263.555	1263.556	-0.65	5.4	164	173	VQE**C**ADILEW	66792
852.448	852.446	1.73	5.2	364	370	EKLQATY	23647
966.491	966.489	2.03	5.1	2362	2370	QALAEGKSY	1717
5788.926	5788.981	-9.48	4.8	1869	1920	AVHETRVQNV**C**AQGEDILNKVLQEESQNKEISSKIEALNEKTPSLAKAIAAW	3774
802.330	802.337	-8.22	4.8	2413	2419	TNSYFGN	5889
1603.711	1603.739	-17.40	4.8	902	914	QQYLADLHEAETW	6290
2193.952	2193.977	-11.35	4.8	466	481	DERHRQYEQ**C**LDFHLF	1892
2065.934	2066.004	-33.71	4.7	1944	1963	IADKETSLKTNGNGADLGDF	6335
950.372	950.392	-21.38	4.6	1090	1097	EAGDMLEW	1078
3284.517	3284.539	-6.43	4.5	1385	1410	EKRKKILDQ**C**LELQMFQGN**C**DQVESW	2553
2727.342	2727.442	-36.73	4.4	1124	1146	QKDLNTNEPRLRDINKVADDLLF	1109

928
929

51

Extended Data Fig. 1

a

r = 0.9532, p<0.0001, n = 258

b

Streptavidin - PE

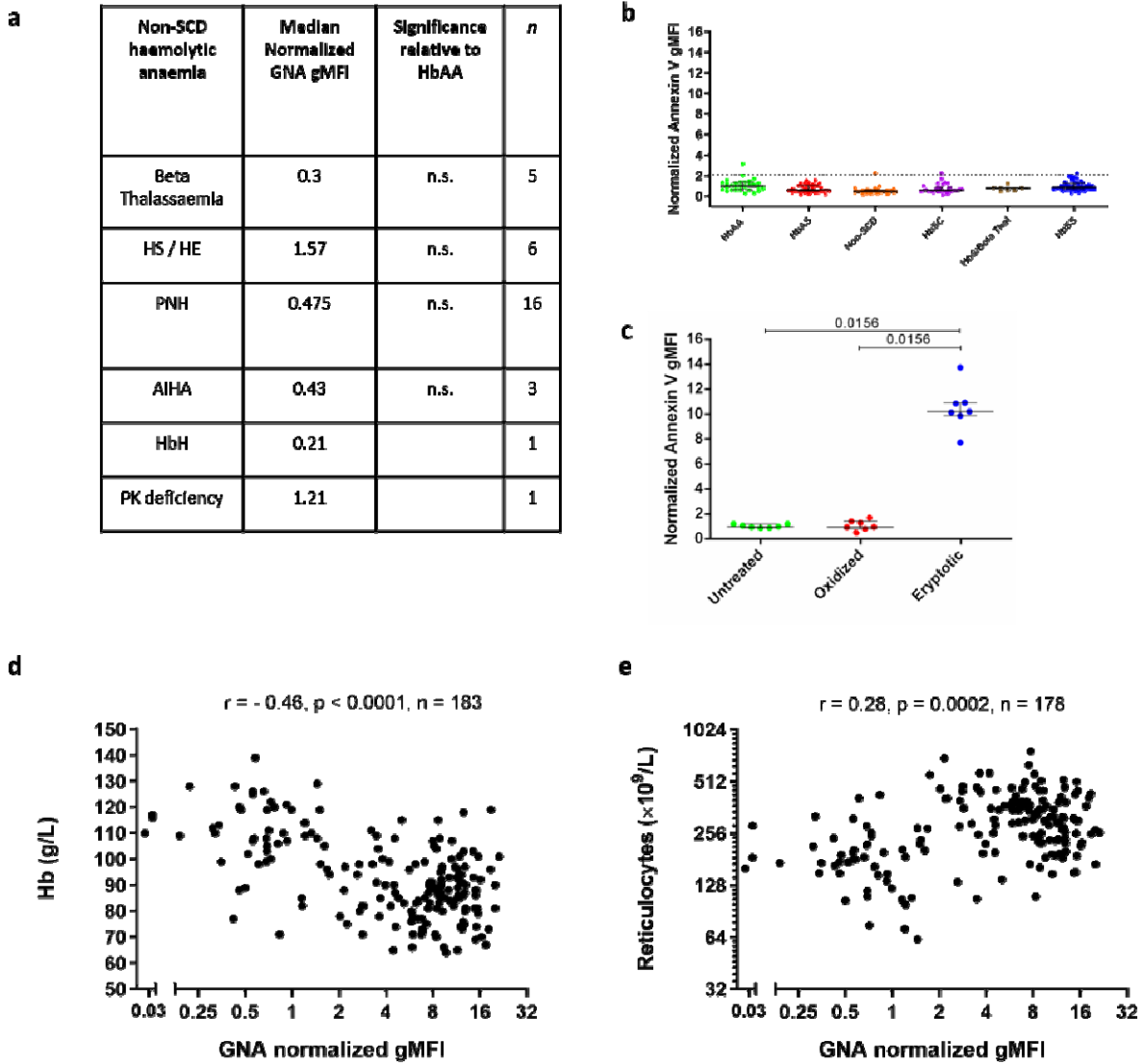**c** GNA/Strep-PE complex   Brightfield   Merge

d

e

930

931   **Extended Data Figure 1: Specificity of binding of mannose binding lectins to RBCs.**

932   a) Correlation of NPL with GNA lectin surface binding; normalized gMFI, Spearman's rank

933   correlation.

934   b) Flow cytometric histograms of GNA lectin and streptavidin control binding for HbSS

935   RBCs with and without mannan blockade. Representative of 3 independent experiments

936   from different donors.

937   c) GNA lectin/Streptavidin PE staining of HbSS RBCs is visualized by fluorescence

938   microscopy (PE alone, Brightfield alone and merge).

939   d) HbSS RBCs from a section of image from c) are counted for the number of GNA lectin

940   binding patches visualized by fluorescence microscopy (left) and plotted on the right.

941   Mean 18.3, SD 8.6.

942   e) Percentage high mannose structures, with respect to total N-glycans. Untreated HbAA (n

943   = 2) and HbSS (n = 5) ghosts are analysed by N-glycome mass spectrometry. Results are

944   pooled from four independent experiments. High mannose and complex N-glycans total

945   100%. Mann Whitney statistical test.

946

Extended Data Fig. 2

a

Non-SCD haemolytic anaemia	Median Normalized GNA gMFI	Significance relative to HbAA	*n*
Beta Thalassaemia	0.3	n.s.	5
HS / HE	1.57	n.s.	6
PNH	0.475	n.s.	16
AIHA	0.43	n.s.	3
HbH	0.21		1
PK deficiency	1.21		1

b

c

d

e

947

54

Extended Data Figure 2: Binding of mannose binding lectins and annexin V to RBCs.

a) Table of normalized gMFI values for GNA lectin binding to non-SCD haemolytic anaemias, Mann-Whitney tests relative to HbAA.

b) Normalized gMFI of annexin V binding to RBCs in whole blood samples. Dotted line shows 90th centile of annexin V staining within HbAA. Non-SCD include haemolytic anaemias listed in Extended Data Fig. 2a. HbAA (n=29), HbAS (n=42), Non-SCD (n=33), HbSC (n=30), HbS/Beta Thal (n=7), HbSS (n=52). No significant differences by Mann-Whitney.

c) Normalized gMFI of annexin V binding to oxidized (copper sulphate/ascorbic acid), eryptotic (calcium ionophore) or untreated purified HbAA RBCs; Wilcoxon.

d) Plots of haemoglobin concentrations,

e) and reticulocyte counts against normalized GNA lectin gMFI for SCD including HbS/B+, HbSC (compound heterozygosity for HbS with β-thalassaemia and HbC respectively) and HbSS patients. Spearman's rank correlation shown.

Extended Data Fig. 3
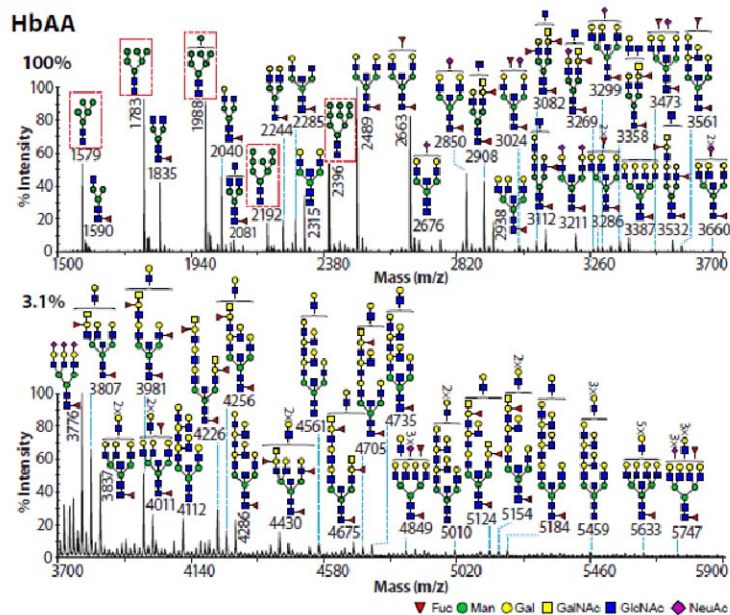
For calculation, upper panel of N-glycans has been taken into account.

High mannose N-glycans: 35.9%
Complex N-glycans: 64.1%
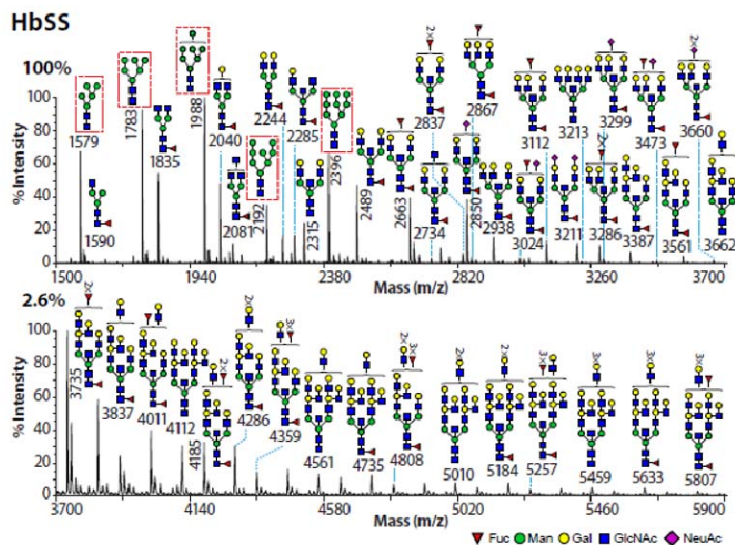
For calculation, upper panel of N-glycans has been taken into account.

High mannose N-glycans: 48.3%
Complex N-glycans: 51.7%

963 **Extended Data Figure 3. Full N-glycome spectra from HbAA and HbSS ghosts.**

964 Spectra from individual HbAA (upper panel) and HbSS (lower panel) ghosts are shown. Zoom

965 factors are indicated by the percentages on top of the intensity axis. For calculations of

966 percentages high mannose and complex N-glycans, the upper panel of each N-glycan profile was

967 used.

968

969

Extended Data Fig. 4
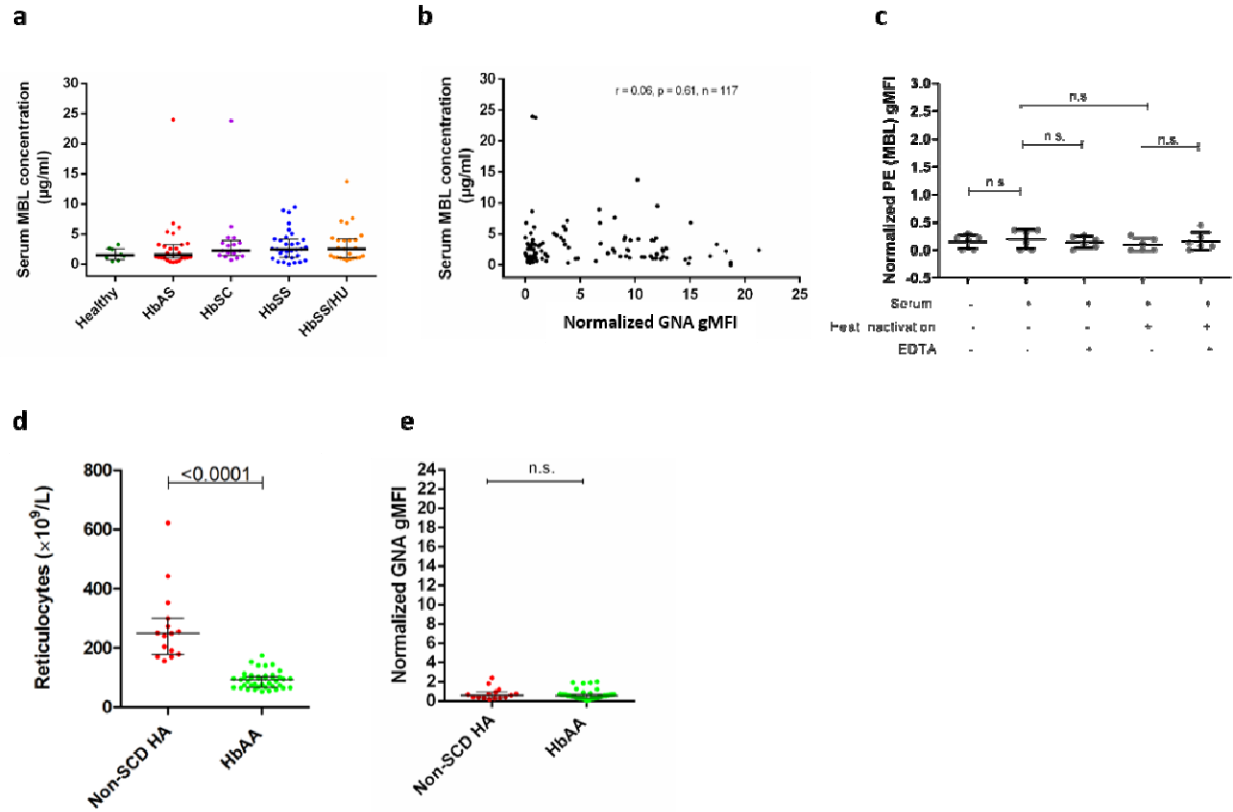
970

971 **Extended Data Figure 4: Mannose binding lectin correlations and stratification of mannose**

972 **relationship to anaemia.**

973 Concentrations of serum mannose binding lectin (MBL): (a) split by clinical phenotype (HbAA

974 (n=8); HbAS (n=27); HbSC (n=17); HbSS (not receive hydroxycarbamide treatment, n=32);

975 HbSS/HU (receiving hydroxycarbamide treatment, n=25), (b) correlation with surface GNA

976 lectin binding and (c) lack of direct binding to HbSS RBCs (n=6). Comparison of reticulocyte

977 counts (d) or normalized GNA lectin binding gMFI (e) between HbAA and non-SCD haemolytic

978 anaemias (Non-SCD HA). For d), HbAA (n=15), non-SCD (n=37). For e), HbAA (n=15), non-

979 SCD (n=41).

Extended Data Fig. 5
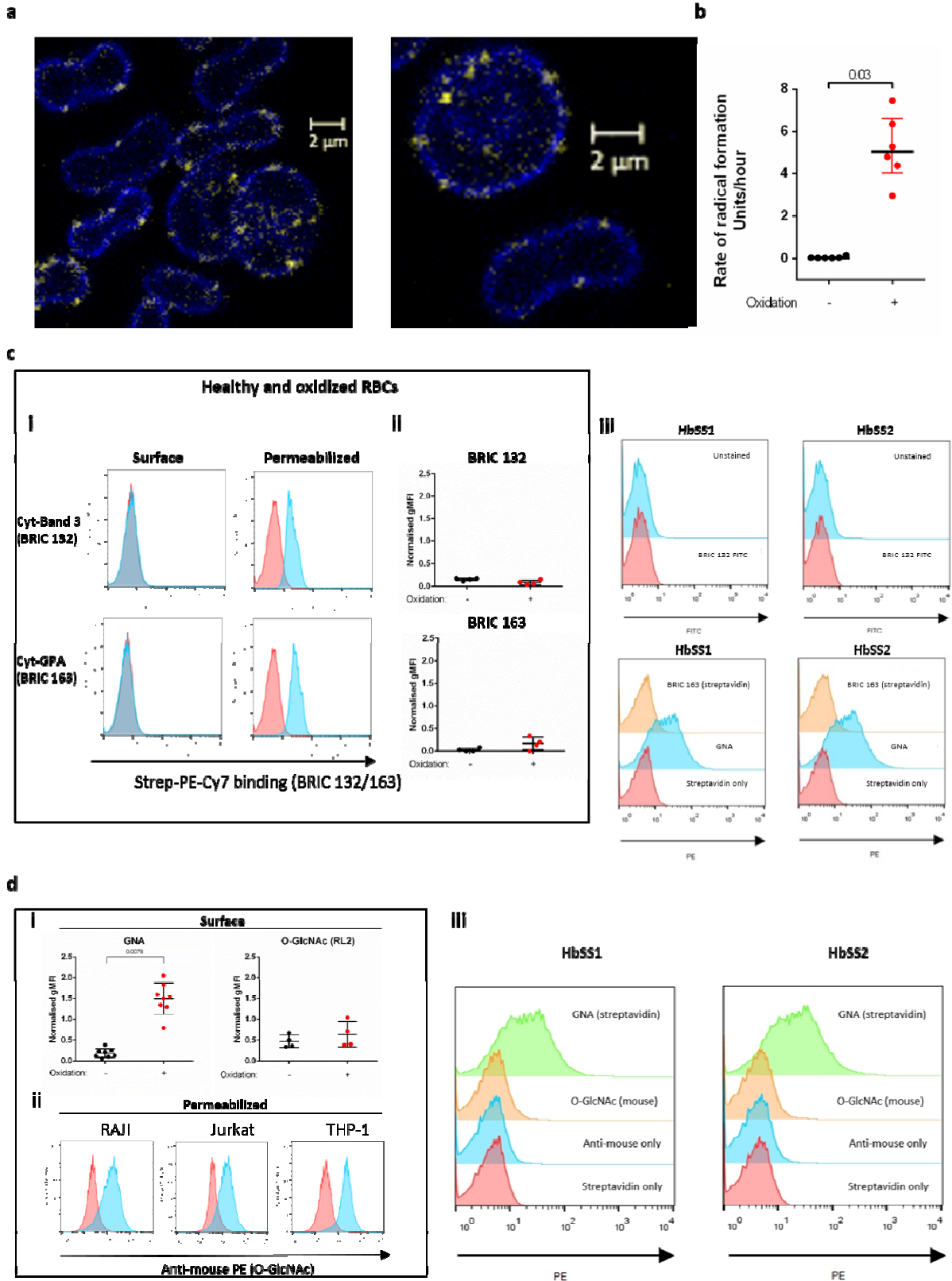
981   **Extended Data Figure 5: Oxidation exposes mannose on the surface of RBCs**

982   a) Confocal microscopy of HbAA RBCs permeabilized before staining with biotinylated

983   GNA lectin, streptavidin (yellow) and anti-spectrin (blue).

984   b) Rate of radical formation calculated from six-hour time course measurement for healthy

985   RBCs with or without oxidation by $CuSO_4$/ascorbic acid during time course.

986   c) Flow cytometric analysis of healthy, oxidized and HbSS RBCs using BRIC 132 (anti-

987   cytoplasmic band 3) or BRIC 163 (anti-cytoplasmic glycophorin A). Left hand panels: i)

988   histograms for permeabilized versus non-permeabilized binding of HbAA RBCs to BRIC

989   antibodies. ii) BRIC antibody binding to surfaces of oxidized and undamaged HbAA

990   RBCs. Differences not significant by Mann-Whitney. Right hand panel (iii): BRIC

991   antibody and GNA lectin binding to RBCs from two HbSS donors, without

992   permeabilization.

993   d) Flow cytometric analysis of healthy, oxidized and HbSS RBC using O-GlcNAc specific

994   antibody, RL2. i) Normalized GNA lectin and RL2 binding for undamaged and oxidized

995   RBCs, without permeabilization. ii) Histograms for RL2 binding to permeabilized

996   nucleated cells shown. Right hand panel (iii): RL2 antibody and GNA lectin binding to

997   RBCs from two HbSS donors, without permeabilization.

998

Extended Data Fig. 6

Two-toned fluorescence phagocytosis (TTFP) assay

a Oxidized RBC (Red) / DAPI (Blue)

b
i GPA-FITC
ii GPA –FITC + CTFR
iii Bright Field
iv Merge

c

d

e
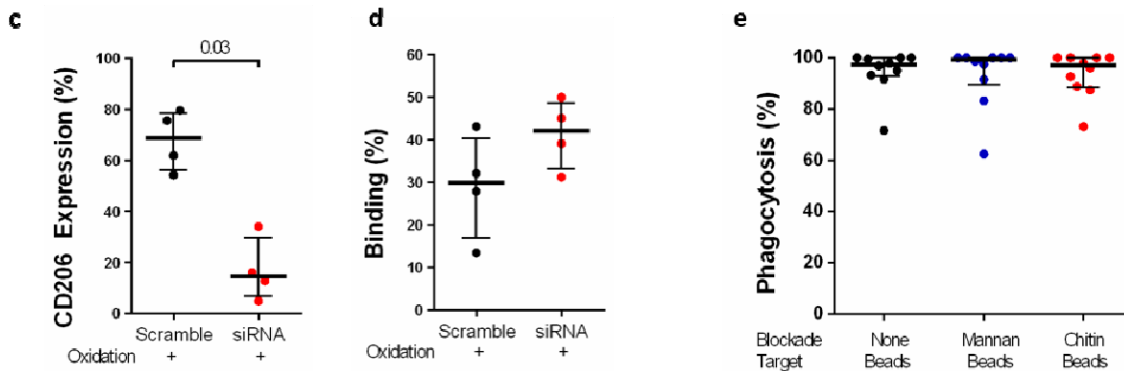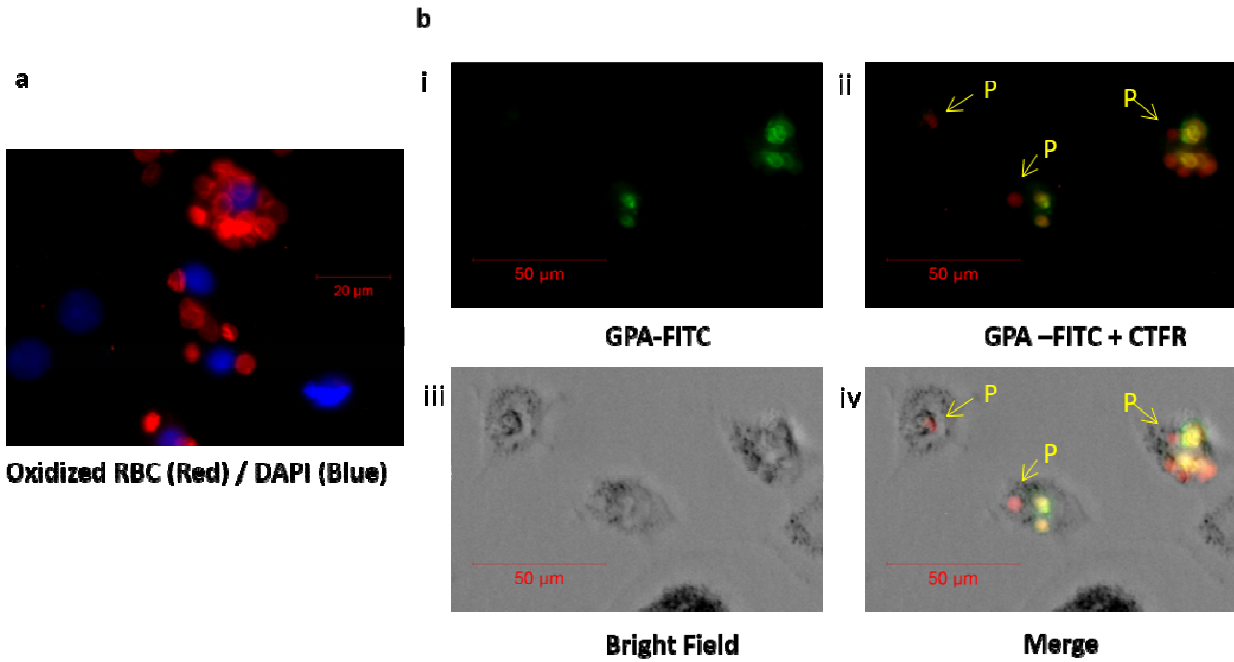
999

1000

1001 **Extended Data Figure 6: Two-toned fluorescence phagocytosis (TTFP) assay**

1002 a) Oxidized RBCs stained with Cell Trace Far Red (CTFR, red) are incubated with HMDM

1003 for 3 hours, washed with PBS, permeabilized and stained for nucleus (DAPI, blue).

1004 Immunofluorescence. Scale bar shown.

1005 b) Oxidized RBCs stained with Cell Trace Far Red (CTFR, red) are incubated with HMDM

1006 for 3 hours, washed with PBS, and counter-stained prior to immunofluorescence

1007 microscopy with anti-GPA-FITC antibody (green) to identify RBCs that are not

1008 sequestered inside macrophages: GPA-FITC only (i), GPA-FITC and CTFR (ii), bright

1009 field only (iii) and merged (iv). CTFR (red) single positive cells are counted as having

1010 been phagocytosed (letter E). Double positive (CTFR and GPA) cells are not counted as

1011 having been phagocytosed, but bound to the macrophage cell surface. Scale bar 50 µm

1012 scale as shown.

1013 c) Mannose receptor (CD206) expression assessed by microscopy for human monocyte

1014 derived macrophages treated with siRNA or scramble control. Mann-Whitney.

1015 d) Percentage surface binding of HbSS RBCs assessed by microscopy for human monocyte

1016 derived macrophages treated with siRNA or scramble control.

1017 e) Quantified phagocytosis beads by HMDM with and without glycan polymer blockade,

1018 applied in the same way and the same concentration as for RBC phagocytosis

1019 experiments.

1020

1021

Extended Data Fig. 7
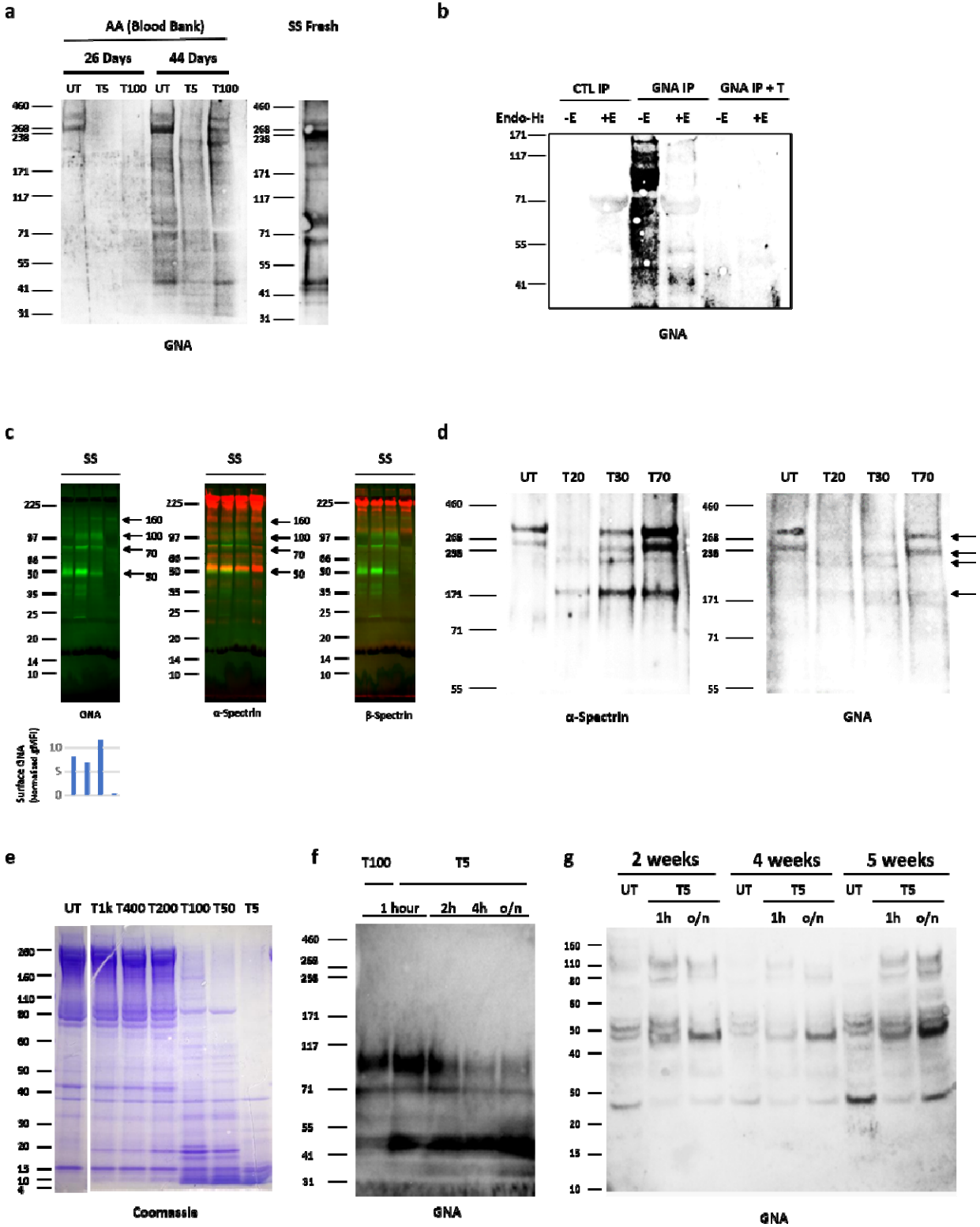
1022

Extended Data Figure 7: High mannose positive fragments derived from aging and proteolysis

a) GNA lectin western from HbAA ghosts isolated from erythrocytes stored from 26 to 44 days. T5 and T100 indicate trypsin digestion of ghosts, where the number indicates the dilution factor of trypsin. Comparison HbSS GNA lectin blot is shown, demonstrating correspondence in the positions of the ~160kDa, ~100kDa, ~70kDa and ~50kDa fragments.

b) Stored RBC (>40 days) ghosts are Triton treated and subjected to GNA lectin precipitation or control (no lectin) precipitation. Endo-H (+E) or control digestion (-E) is applied to the eluates. Overnight trypsin treatment is also applied to a subset of GNA IP elution (GNA IP + T), prior to Endo-H or control digestions.

c) Dual colour western blot from HbSS ghosts using GNA lectin (green) with either α-spectrin or β-spectrin antibodies (both red). Below are corresponding surface FACS GNA lectin staining (normalized gMFI). N.B. The 8-18% gradient gel used here does not yield bright 260kDa GNA lectin binding bands.

d) Partial trypsin digestion of HbAA ghosts (T70 indicates 1:70 ratio of trypsin to sample, etc) then blotted with polyclonal α-spectrin antibody or GNA lectin.

e) Coomassie stain of spectrin released from HbSS ghosts after digestion with trypsin for one hour. Untreated (UT), Tx indicates the dilution factor of trypsin relative to spectrin material.

f) GNA lectin blot of HbSS ghost after prolonged trypsin treatment from 1 hour to overnight (20hours).

65

1045   g) GNA lectin blot of ghosts made from HbSS erythrocytes aged from 2 to 5 weeks.

1046   Untreated (UT), one hour (1h) and overnight (o/n) high concentration trypsin digestions

1047   (T5).

Extended Data Fig. 8
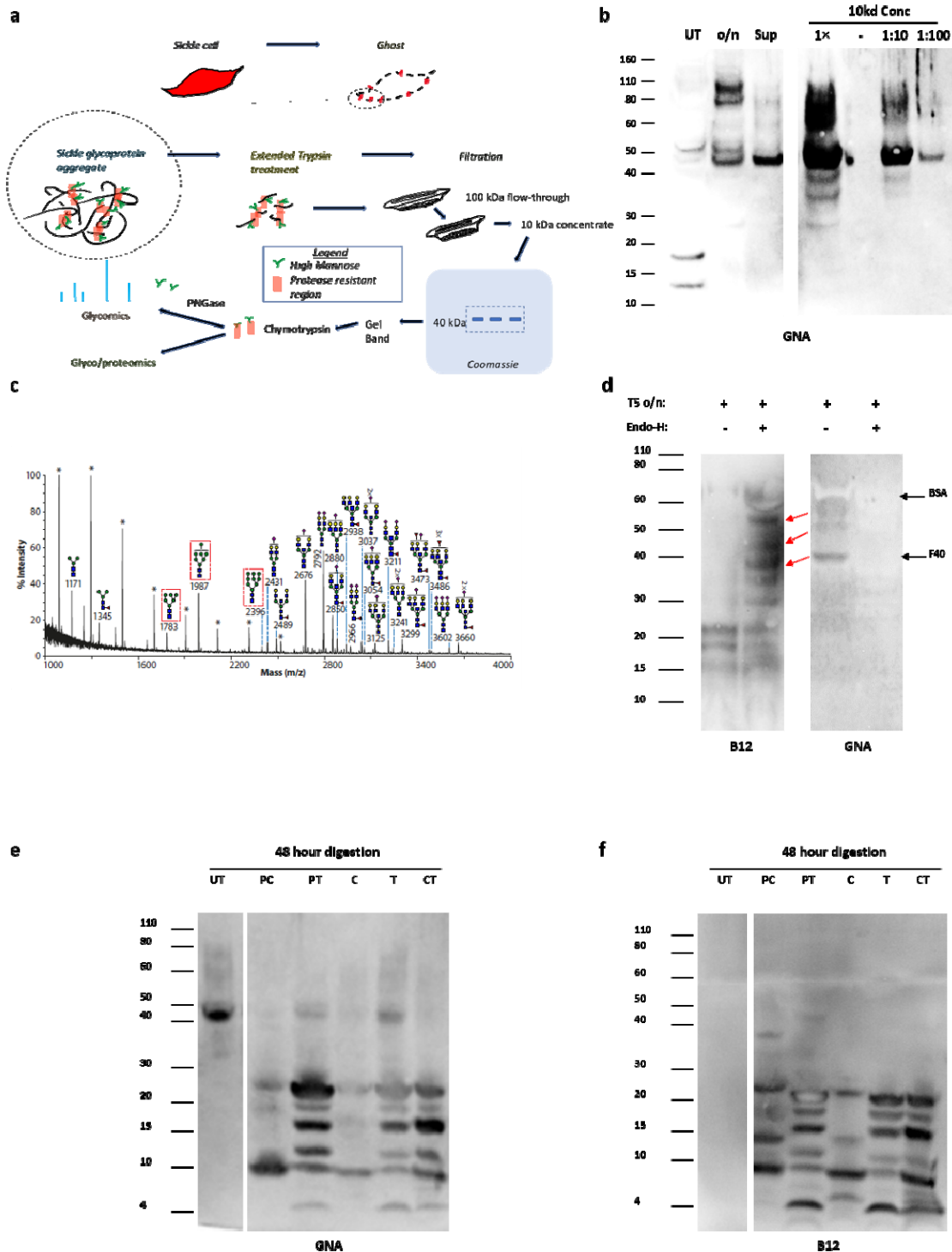
1048

Extended Data Figure 8: Purification and analysis of protease resistant F40 from sickle cells.

a) Cartoon outlining purification process for peptide F40. Sickle cells (top right) are used to make RBC ghosts, which are then subjected to prolonged incubation with trypsin before removing the ghosts by centrifugation. The supernatant is then passed through a 100 kDa filter and concentrated on a 10 kDa filter before running on a polyacrylamide gel. The ~40 kDa band is cut out and digested with chymotrypsin (then PNGase)before analysis by mass spectroscopy for glycopeptides (and glycans).

b) GNA lectin blot of enrichment process of F40 from aged HbSS erythrocyte ghosts. Untreated (UT); overnight T5 (o/n); supernatant from heat inactivated o/n sample (Sup). Final product from sequential concentration with 100kDa and 10kDa concentrators is shown as 1×, 1:10 and 1:100 dilution series. See explanatory notes below.

c) Glycomic analysis following PNGase release of N-linked glycans from F40. Red boxes indicate high mannoses. Putative structures based on composition, tandem MS and biosynthetic pathways. All ions are $[M+Na]^+$. Peaks annotated with an asterisk (*) do not correspond to glycan structures. Major structures are annotated for clarity.

d) HbSS 10kDa concentrate (from a) was digested with trypsin (T5) overnight, heat inactivated, then digested with Endo-H or control for 24 hours. GNA lectin and B12 western blots. Red arrows show likely migration of GNA lectin and B12 reactive bands. Black arrows indicate contaminating BSA and position of F40.

e) HbSS 10kDa concentrate (from a) subjected to combinatorial protease digestion in mild denaturing conditions over 48 hours. Western blot with GNA lectin. (UT) untreated, (PC) pepsin 24 hours then chymotrypsin 24 hours, (PT) pepsin 24 hours then trypsin 24 hours, (C) chymotrypsin 48 hours, (T) trypsin 48 hours, (CT) chymotrypsin 24 hours then trypsin 24 hours, with heat inactivation at 24 hours.

1074   f)   As d) but with western blotting using antibody B12.

1075   **Purification and properties of F40:** F40 from overnight trypsin digestion of HbSS RBC

1076   ghosts partitions to the supernatant following heat inactivation (a). We thereby concentrated

1077   F40, through sequential 100kDa and 10kDa cut off concentrators, by approximately 50-fold

1078   (a). This preparation exhibited remarkably high GNA lectin binding, approximately 100-fold

1079   greater than full length spectrin. Sufficient F40 was purified for glycoproteomic analysis.

1080   PNGase released glycans including three high mannoses, a tri-mannose structure and other

1081   complex glycans (b). The Endo-H sensitive nature of F40 GNA lectin binding restricts the

1082   GNA lectin ligands within this pool of structures to the high mannoses: $Man_6GlcNAc_2$,

1083 $Man_8GlcNAc_2$ and $Man_9GlcNAc_2$. GNA lectin reactivity to F40 shows partial sensitivity to

1084   digestion with chymotrypsin and proteomic analysis of this digest showed the main protein

1085   represented was α-spectrin (Fig. 4i). The most abundant peptides came from the N-terminal

1086   370 amino acids, spanning spectrin repeats 1 to 3, with only scattered, low abundance

1087   peptides identified from the rest of the molecule and none from β-spectrin. Excluding mass

1088   spectrometry incompatible regions from this region yielded 34% coverage across spectrin

1089   repeats 1 to 3, with 64% coverage within repeat 3.

1090   Identification of the N-terminal portion of α-spectrin as a major constituent of F40 from mass

1091   spectrometry analysis was also supported by western blotting using B12, an N-terminus

1092   specific α-spectrin antibody. The antibody does not bind GNA lectin reactive F40 or two

1093   higher molecular weight bands directly, but epitopes are revealed by removal of high

1094   mannoses using Endo-H (c). Furthermore, three new B12-binding bands migrated at a

1095   slightly lower positions relative to the three GNA lectin binding bands, consistent with

1096   glycosidase induced cleavages (c). 48 hour-long digestions with combinations of proteases

69

1097   were able to cleave F40 and, even without Endo-H treatment, unmask B12-binding epitopes

1098   (e). The GNA lectin and B12-binding fragments align remarkably well under all treatment

1099   combinations (d, e). These data suggest the high mannose decoration and unusual protein

1100   structure of F40 limits antibody access and may account for its resistance to proteases.

1101

Extended Data Fig. 9
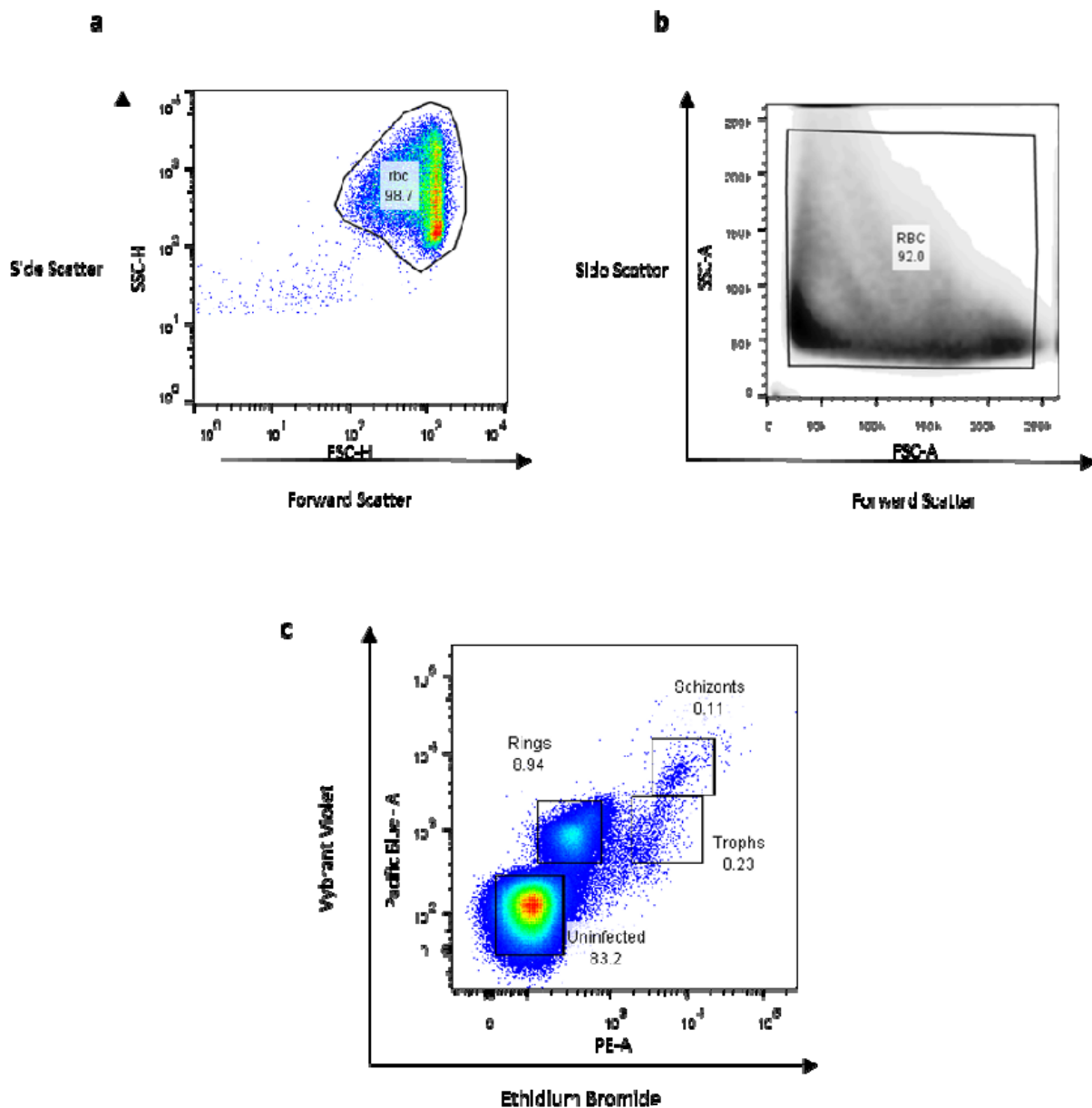
1102

1103   **Extended Data Figure 9. Gating strategy for flow cytometric analysis.**

1104   a) Example of gating strategy for selecting whole red blood cells used in both whole blood

1105   and purified RBC flow cytometry (with the exception of *P. falciparum* infected RBC

1106   flow cytometry).

1107   b) Example of first gating of whole red blood cells used in analysis of *P. falciparum*

1108   infected RBC flow cytometry.

1109   c) Example of second gating of *P. falciparum* infected RBCs by maturation stages as

1110   defined by ethidium bromide (PE) and Vybrant Violet (Pacific Blue) staining.

1111